UNIVERSITÀ DEGLI STUDI DI PALERMO

Dottorato di Ricerca in Scienze Agrarie, Alimentari, Forestali e Ambientali
Dipartimento di Scienze Agrarie, Alimentari e Forestali
SSD AGR/08

EXPERIMENTAL STUDY OF RILL FLOW RESISTANCE AT PLOT SCALE

IL DOTTORE
ALESSIO NICOSIA

IL COORDINATORE
CHIAR.MO PROF. VINCENZO BAGARELLO

IL TUTOR
CHIAR.MO PROF. ING. VITO FERRO

IL COTUTOR
ING. VINCENZO PAMPALONE

CICLO XXXIII
ANNO CONSEGUIMENTO TITOLO 2021

DOTTORATO

Index

I. Extended Abstract

Erosive processes are a relevant environmental problem of our society. In fact, these processes have many consequences reducing the soil fertility and productivity, worsening air and water quality and impacting the biodiversity reducing the variety of communities. Water erosion is one of the most determining phenomena regarding soil erosion and soil loss. Soil loss due to water erosion is a natural and inevitable phenomenon, but it can become intolerable in particular conditions often determined by anthropic factors (Di Stefano and Ferro, 2016).

Water erosion processes are generally characterized as either interrill or rill erosion. On interrill areas, characterized by spread flow (overland flow), the main erosion process is due to raindrop impact, and the sediment is transported by flow from these areas to rills. Instead, rills are small, shallow, and ephemeral flow paths which work as sediment sources and are able to transport particles delivered from interrill areas and those detached by rill flow along the rill wetted perimeter (Di Stefano et al., 2013). Rill erosion is the main sediment source at hillslope scale and more than 80% of the eroded particles from hillslopes are transported in rills (Mutchler and Young, 1975).

The study of the physical processes and mechanisms which determine water erosion becomes a fundamental tool to understand in a better way the problem, estimate the soil loss and try to manage it. The rill erosion strictly depends on hydraulic characteristics of the flow which moves within the rill (Foster et al., 1984) and for this reason to study and model rill erosion processes, in addition to flow discharge Q, other hydraulic characteristics, as width w, water depth h, mean flow velocity V, and roughness coefficient, must be defined (Gilley et al., 1990).

One of the most common available approach to estimate the mean flow velocity in rills, notwithstanding the difference between them and rivers, is the use of classical hydraulic equations, such as Manning's and Chezy's equation.

In this dissertation experimental investigations were carried out to determine the rill flow resistance law, analyzing the behavior and the contribution to the total resistance of the *grain* component, due to the characteristic dimension of the elements which determine bed roughness, *morphological* resistance, due to bed forms as step-pools, and the resistance related to sediment transport phenomena.

A theoretical flow resistance law was deduced integrating a power flow velocity profile (Ferro, 1997, 2003), obtained applying the dimensional analysis (Barenblatt, 1993; Ferro,

1997) and the self-similarity hypothesis (Ferro and Pecoraro, 2000; Di Stefano et al., 2017b; Ferro, 2017).

Rills were manually shaped on plots and deepened by a clear flow and experimental runs were carried out on rill reaches to measure mean flow velocity, water depth, cross-section area, wetted perimeter, and channel slope. An image-based technique, which couples Structure from Motion (SfM) and Multi-View Stereo (MVS), was applied for obtain the ground measurements by 3D models. The plots were filled with five different soil types, the plot slopes s_p varied from 9 to 26%, and both mobile and fixed bed conditions were examined.

Using the obtained measurements three analyses were developed.

For the first investigation 472 experimental runs, characterized by different soil textures and slopes, were used to calibrate and test the equation to estimate the Γ function of the velocity profile and consequently obtain the flow resistance law. The different soil textures were represented by clay and silt percentage. The analysis demonstrated that clay and silt fractions of the investigated soils are sufficient for representing the effect of erosion and transport of soil particles on rill flow velocity. In fact, the friction factor increases when silt fraction increases (high detachability) and clay fraction decreases (low transportability). In other words, this result expresses that the increase of flow resistance due to *sediment load* is affected by both soil detachability and transportability.

The second investigation, carried out using 199 experimental runs for which step-pools occurred, allowed to calibrate and test the equation to estimate the Γ function for both mobile and fixed bed rills characterized by the occurrence of the *morphological* resistance. The equation calibrated by mobile bed rills is applicable to the fixed bed condition and this result is explainable since the effect of sediment transport on the flow resistance law can be considered negligible respect to the form-induced flow resistance (spill resistance) due to the presence of step-pools structures. The analysis confirmed that the step-pool configuration is characterized by Darcy-Weisbach friction factor values higher than those obtained for rills with a flat bed.

The aim of the third and last analysis was to evaluate the contribution of the resistance due to sediment transport on total one comparing the runs carried out on mobile and fixed bed rills for two different databases. For these experimental conditions this type of resistance resulted often negligible.

The theoretical approach resulted successful and was characterized by low errors in the estimate of the Darcy-Weisbach friction factor for the three conducted analyses.
In all cases the "feedback mechanism" hypothesis suggested by Govers (1992), for which the mean flow velocity is independent by the slope gradient, was confirmed. For fixed bed runs this result can be justified by a "frozen" feedback caused by mobile bed runs before fixing operations or by the shaping phase.
In conclusion, the estimate of the Γ function of the velocity profile and the application of the theoretical flow resistance is successful and reliable for both *grain* and *morphological* resistance and is also useful to investigate sediment transport effects.

II. Sommario Esteso

I processi erosivi costituiscono un rilevante problema ambientale con impatto anche di tipo socioeconomico. Infatti, questi processi determinando l'asportazione degli strati superficiali di suolo, causano la riduzione della fertilità e produttività del suolo, e hanno un considerevole impatto sulla biodiversità. La perdita di suolo dovuta all'erosione idrica è un fenomeno naturale ed inevitabile, che può divenire intollerabile in condizioni particolari che spesso dipendono da fattori antropici (Di Stefano e Ferro, 2016).
I processi di erosione idrica sono generalmente caratterizzati dall'erosione interrill o rill. Nelle aree interrill, caratterizzate da correnti overland, il processo erosivo preponderante è dovuto all'impatto delle gocce di pioggia, e il sedimento viene trasportato dalla corrente da queste aree verso i rill. I rill, invece, sono solchi di modeste dimensioni planimetriche, poco profondi ed effimeri, che operano come principale sorgente di sedimento, in cui vengono trasportate le particelle provenienti delle aree interrill e quelle distaccate dalla superficie laterale del rill stesso (Di Stefano et al., 2013). L'erosione rill rappresenta la principale fonte di sedimento a scala di versante dato che più dell'80% delle particelle erose nei versanti è trasportato nei rill (Mutchler e Young, 1975).
Lo studio dei processi fisici e dei meccanismi che determinano l'erosione idrica risulta necessario per meglio comprendere il fenomeno erosivo e per stimare i valori di perdita di suolo. L'erosione rill dipende strettamente dalle caratteristiche idrauliche della corrente che muove all'interno del rill (Foster et al., 1984), per cui al fine di studiare e modellare i processi erosivi, oltre alla portata Q, devono essere determinate altre caratteristiche idrauliche, come la larghezza w, il tirante idrico h, la velocità media della corrente V, e l'indice di scabrezza (Gilley et al., 1990).

Nonostante le differenze tra i rill e i corsi d'acqua, uno degli approcci più comuni per la stima della velocità media della corrente nei rill è basato sull'utilizzo delle equazioni dell'idraulica classica, come quelle di Manning o di Chezy.

Nella presente Tesi sono presentati i risultati di sperimentazioni condotte per la determinazione della legge di resistenza al moto nelle correnti rill. È stato, inoltre, analizzato il contributo alle resistenze totali della componente *grain*, dovuta alla dimensione caratteristica degli elementi che determinano la scabrezza, della *morphological* resistance, dovuta alle forme di fondo come gli step-pool, e della resistenza dovuta al trasporto solido.

Una legge teorica di resistenza al moto è stata dedotta a partire dall'integrazione del profilo potenziale di velocità della corrente (Ferro, 1997, 2003), ottenuto applicando l'analisi dimensionale (Barenblatt, 1993; Ferro, 1997) e l'ipotesi di auto-similitudine incompleta (Ferro e Pecoraro, 2000; Di Stefano et al., 2017b; Ferro, 2017).

I rill sono stati incisi manualmente su due parcelle, modellati con una corrente limpida e le prove sperimentali sono state condotte in tratti di rill al fine di misurare la velocità media della corrente, il tirante idrico, l'area delle sezioni trasversali, il contorno bagnato e la pendenza del tratto. Un metodo di rilievo di tipo *image-based*, che combina le tecniche Structure from Motion (SfM) e Multi-View Stereo (MVS), è stato applicato per realizzare il modello 3D dei rill. Sono stati utilizzati cinque differenti tipi di suolo, con pendenza variabile tra il 9 e il 26%, e sono state eseguite prove sia a fondo mobile che fisso.

Le misure ottenute hanno consentito di sviluppare tre differenti analisi.

Per la prima analisi sono state utilizzate 472 misure sperimentali, caratterizzate da differenti tessiture del suolo e pendenze della parcella, per calibrare e verificare l'equazione per la stima della funzione Γ del profilo di velocità e determinare, conseguentemente, la legge di resistenza al moto. Nella relazione proposta, la tessitura è rappresentata dal contenuto percentuale di argilla e limo. L'analisi ha mostrato che sia la frazione argillosa che quella limosa, rappresentative della distaccabilità e trasportabilità delle particelle di suolo, condizionano la velocità media della corrente rill. Infatti, l'indice di scabrezza aumenta all'aumentare della frazione limosa (elevata distaccabilità) e al diminuire della frazione argillosa (bassa trasportabilità). In altri termini, il risultato ottenuto dimostra che l'incremento di resistenza al moto dovuto al carico solido è influenzato sia dalla distaccabilità che dalla trasportabilità delle particelle di suolo.

La seconda analisi, condotta utilizzando 199 misure sperimentali ottenute in presenza di step-pool nei rill, ha permesso di calibrare e verificare l'equazione per la stima della funzione Γ sia per rill a fondo mobile che per rill a fondo fisso. L'equazione calibrata per i rill a fondo mobile è risultata applicabile anche alle misure ottenute su fondo fisso perché l'effetto del trasporto solido sulle resistenze al moto può essere ritenuto trascurabile rispetto alle resistenze dovute alla morfologia a step-pool. La configurazione di rill con step-pool è risultata caratterizzata da valori dell'indice di resistenza di Darcy-Weisbach più elevati di quelli ottenuti per rill a fondo mobile senza forme di fondo.

Lo scopo della terza ed ultima analisi è stato quello di valutare il contributo della resistenza al moto dovuta al trasporto solido rispetto alla resistenza totale utilizzando le misure effettuate su rill a fondo piano, sia mobile che fisso per due differenti database. Per le condizioni sperimentali esaminate questo tipo di resistenza è risultata spesso trascurabile.

Per le tre analisi effettuate, l'approccio teorico è risultato applicabile in quanto sono stati ottenuti bassi valori degli errori nella stima dell'indice di resistenza di Darcy-Weisbach.

In tutti i casi esaminati l'ipotesi del meccanismo "feedback" proposta da Govers (1992), per la quale la velocità media della corrente è indipendente dalla pendenza, è stata confermata. Per le prove effettuate su rill a fondo fisso questo risultato può essere spiegato da un effetto feedback "memorizzato", determinato dalle prove a fondo mobile effettuate prima delle operazioni di irrigidimento dei solchi o dalla fase di modellamento.

In conclusione, la stima della funzione Γ del profilo di velocità e la conseguente applicazione della legge teorica di resistenza al moto è risultata affidabile sia nel caso di rill a fondo piano (*grain resistance*), sia nel caso di rill con step-pool (*morphological resistance*). La suddetta equazione ha consentito anche di valutare l'effetto del trasporto solido sulla resistenza al moto della corrente rill.

1. INTRODUCTION

1.1. *Soil erosion: a global environmental problem*

Nowadays worldwide people are more and more becoming aware of the environmental problems which afflicts our society and jeopardize the future world and its sustainability for us and the following generations. Politicians, social media, journalists, and activists talk every day about environmental problems as the global warming, the climate change, the ice melting in the Arctic, the Earth Overshoot Day (when humanity's demand on nature exceeds what Earth's ecosystems can renew and produce in a year), etc., but often other problems tend to be underrated. In fact, problems as land degradation, soil loss and erosion, decrease of soil fertility and productivity are scarcely considered among the population and this is probably due to a lack of public consciousness about these themes. People think that the soil is a renewable resource, but it is not. The soil formation is a long-lasting process which requires hundreds of years to be ended and this seems contradictory looking at the relentless and exaggerated mistreatment of lands. In addition, environmental and landscape protection is often inadequate and interventions to prevent damages, or sometimes catastrophes, due to hydrogeological instability are scarce.

Land degradation processes have many consequences reducing the soil fertility and productivity, worsening air and water quality and impacting the biodiversity reducing the variety of communities (plants, animals, etc.). According to FAO report (Gomiero, 2016), about the 25% of the global lands are recognized as “highly degraded” and most of land degradation is due to soil erosion phenomena, especially in the less populated area. Joint Research Centre (JRC) estimated that in Europe soil erosion affects over 12 million hectares of land and leads to €1.25 billion loss in crop productivity.

In particular, water erosion (Figure 1) is one of the most determining phenomena regarding soil erosion and soil loss. Soil loss due to water erosion is a natural and inevitable phenomenon, but it can become intolerable in particular conditions often determined by anthropic factors (Di Stefano and Ferro, 2016).

The mean soil loss rate due to water erosion in the European Union's lands (Figure 2) (agricultural, forests and semi-natural areas) was found to be 2.46 t ha^{-1} yr^{-1} in 2010, resulting in a total soil loss of 970 Mt annually (Panagos et al., 2015). The seriousness of this problem is highlighted by the fact that the average rate of soil formation in Europe is 1.4 t ha^{-1} yr^{-1} (Verheijen et al., 2009). About 77% of Italian soils are at risk of accelerated

water erosion (Gazzolo and Bassi, 1961) and the mean soil loss is 7.4 t $ha^{-1}yr^{-1}$ (Stolte et al., 2016).

Figure 1. Example of water soil erosion.

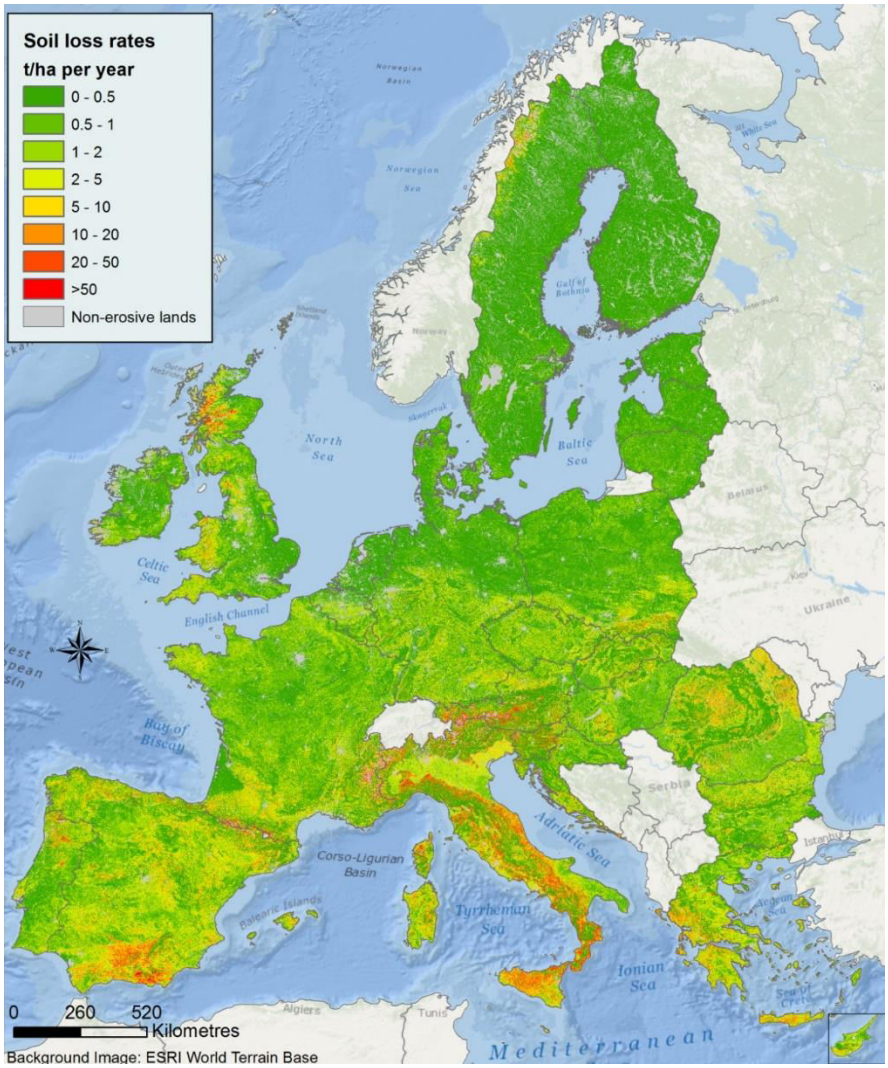

Figure 2. European map of soil loss by water erosion (source: JRC, ESDAC).

During last years, politics tried to focus on this relevant problem, drawing up, for instance, the rural development programme at regional scale. These measures try to increase the awareness of farmers, public institutions, and local politicians with the common aim to reach a sustainable management of agricultural lands and forests. These interventions, suggested by EU, helped to contrast the erosive phenomena but it is not still enough. In fact, in the last decade in Europe soil erosion reduced by 9.5%, but 13% of the cultivated lands still have a soil loss higher than 5 t $ha^{-1}yr^{-1}$. In particular, in Sicily the majority of agricultural lands presents a soil loss higher than 5 t $ha^{-1}yr^{-1}$ and sometimes enormous values in order of 20-25 t $ha^{-1}yr^{-1}$. The main problem of this region is that erosive events (i.e., natural events producing measurable runoff) occur mainly during the fall-winter interval, that corresponds to the period in which soils are often uncovered and consequently more erodible. Furthermore, in many natural hillslopes the vegetation is absent or sparse and, as it is known, plants introduce a series of advantages that considerably reduce erosion processes. Starting from the bottom, the presence of roots increases the cohesion of the soil and the aggregation of soil particles, physically reinforcing the shear zone (Stokes et al., 2009), and indirectly increasing the content of organic matter and improving the soil structure, through litter and plant root turnover (Angers and Caron, 1998), root exudates and rhizodeposition (Gyssels et al., 2005; Pohl et al., 2009). Soil organic carbon produced by decomposition of the roots allows transformation of the micro-aggregates into macro-aggregates (> 250 μm up to several mm diameter) (Gale et al., 2000; Wander and Yang, 2000). At the surface, plants can mitigate the raindrops effects by covering the soil with their canopy, plant basal areas, and dropped litter, consequently greatly reducing the detachment due to the raindrop impact. Lastly, the presence of vegetation creates a further obstacle to runoff, increasing considerably the flow resistance. In fact, the presence of stems and grass on topsoil decreases flow velocity, thus diminishing flow transport capacity.

Water erosion processes include the *detachment* of the soil particles, their incorporation into the flow (*entrainment*), their *transport* and their *deposition*. The transported particles, elementary or aggregate, are called *sediments*. Water erosion is caused by shear stress on soil surface, determined by the rainfall impact and the surficial flow originated by a weather event or by irrigation. Erosive phenomena also strictly depend on soil characteristics, as the attitude of the soil particles to be detached (*detachability*) and to be transported (*transportability*). In fact, greater and heavier particles (sand) are easily

detachable but hard to transport. Another important variable is the transport capacity of the flow, which is the maximum amount of sediment with given characteristics (dimensions, specific weight) that can be transported and depends on flow hydraulic characteristics (water depth, discharge, etc.).

Studying the water erosion, the reference spatial unit is the watershed. The surficial flow can move both diffusely and channelized in rills, gullies or hydrographic network.

Erosion by rainfall and runoff is a major driver in landscape evolution. Water erosion processes are generally characterized as either interrill or rill erosion, which behave differently. On interrill areas, characterized by spread flow (*overland flow*), shallow water depth and low bed shear stress (Mutchler and Young, 1975; Toy et al., 2002), the main erosion process is due to rain splash, whereas the transport of detached sediments to rills is due to overland flow. Instead, rills are small, shallow, and ephemeral flow paths (Figure 3), which work as sediment sources and can transport particles delivered from interrill areas and those detached by rill flow along the rill wetted perimeter (Bagarello et al., 2015; Bagarello and Ferro, 2004, 2010; Bruno et al., 2008; Di Stefano et al., 2013, 2015). According to Mutchler and Young (1975) (Zhang et al., 2016) more than 80% of the eroded particles from hillslopes are transported in rills, i.e., rill erosion is the main sediment source at hillslope scale.

Figure 3. View of a landscape affected by rill erosion.

1.2. *Rill erosion*

The rill formation and evolution depend on microtopography of the soil surface, and for this reason rills can be removed by ordinary tillage. In addition to the geometry of the soil surface, the formation of rills can be influenced by obstacles, as rock fragments, plants, or

vegetal residuals, which cause the channelization of the flow. Hauge (1977) suggested a cross-section threshold between *rills* and *gullies* equal to 929 cm^2.

For rills, erosive processes can be *detachment-limited* or *transport-limited*. For instance, in a uniform hillslope with several rills usually deposition phenomena do not occur, and the process is controlled by detachment phenomena (*detachment-limited*). On the other hand, if the sediment delivered from the interrill areas exceeds the transport capacity of the channelized flow, deposition phenomena occur (*transport-limited*). This happens, for example, if the slope, and consequently flow velocity, decreases.

Rill formation is due to the head cut migration upstream (Bennett, 1999) and enlargement of the cross-section. The head cut, which can look like a jump (*knickpoint*) (Figure 4) or a sloped flat surface, is an area particularly subjected to erosive phenomena in dependence of soil erodibility, slope of the upstream area and flow discharge.

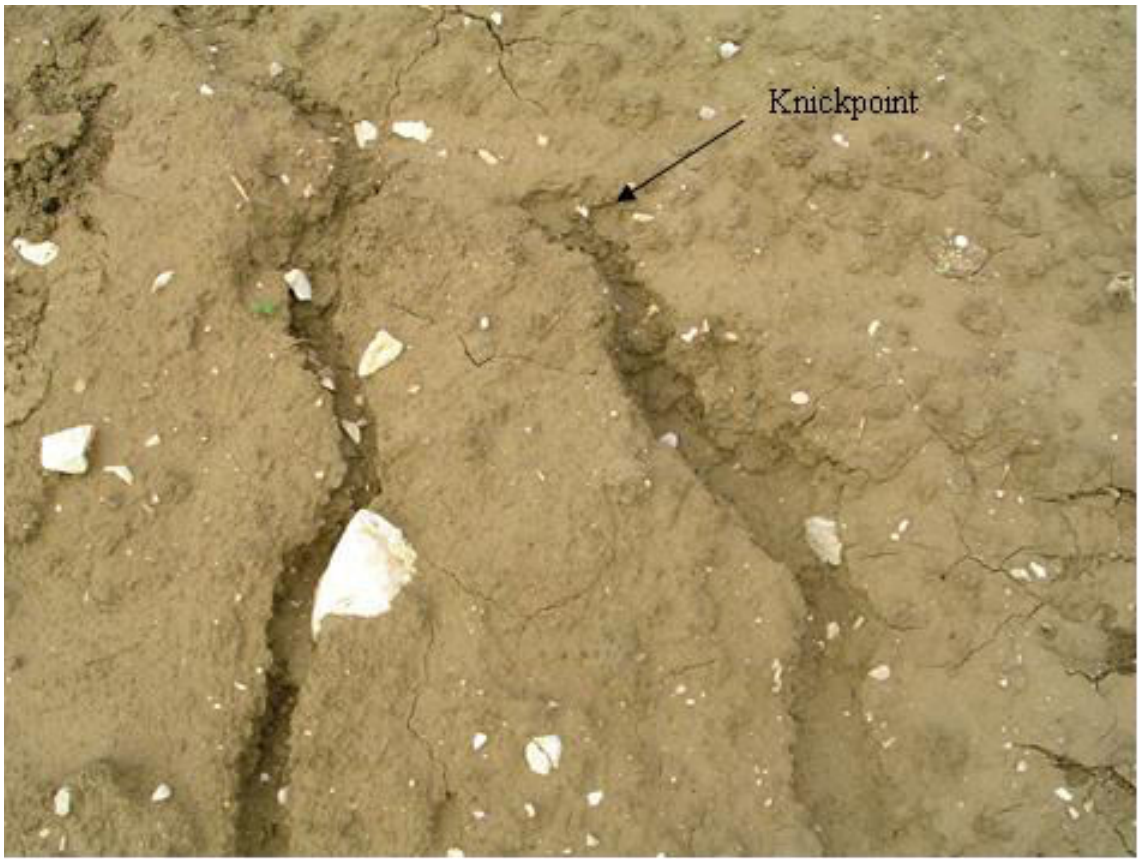

Figure 4. View of a knickpoint.

Also, the formation of tributary is controlled by the formation of the *knickpoint* (Brunton and Bryan, 2000). In fact, when the head cut of the main channel migrates upstream until the point in which overland flows enter the channel from interrill areas, the quote variation determines an increase of the local slope and consequently an increase of the local flow

velocity of the interrill flow. If the flow velocity exceeds the threshold value necessary to detach the particles, other *knickpoints* occur. These *knickpoints* migrate upstream producing the formation of tributary, while the head cut of the main channel continues to migrate upward.

Rill deepening occurs if the flow shear stress, for a fixed mean value in a rill reach characterized by the slope *s*, assumes its maximum value in correspondence of the channel axis. For cohesive soils, the flow determines a deepening but not a width enlargement, which is caused by the boundaries collapse. Rill shape changes during rainfall events. In particular, for low or moderate values of rainfall intensity, the sediment delivered from interrill areas exceeds the transport capacity of the rill flow and consequently, deposition phenomena occur causing the reduction of the section (*network shrinkage*). Instead, for long or high-intensity rainfall events, the transport capacity exceeds the amount of sediment delivered from interrill areas and consequently the flow erodes and enlarges the channel (*network expansion*).

Considering that rills are typically identified by flow depths, which are of the order of millimeters to several centimeters, a large-scale roughness condition can occur. Furthermore, the effect of bed topography, also characterized by steep slope values, on flow hydraulics has to be considered (Abrahams et al., 1996; Foster, et al., 1984; Gilley et al., 1990; Govers, 1992; Nearing et al., 1997; Peng et al., 2015).

Unlike rivers, rills are actively eroded channels and evolve morphologically over a short timescale. Rill morphology results from changes in channel width, flow depth, and bed roughness, which are caused from the eroding action of flow discharge on both bed material and the initial rill structure. In other words, the evolution of the erosion process is due to the interaction among initial rill morphology, flow, and sediment transport. According to Giménez and Govers (2001), the hydraulic conditions in rills should be the result of an equilibrium between the erosive flow and the resistance offered by soil; this hydraulic behavior can be considered similar to a regime channel (Yalin, 1992) allowing to apply a power relationship relating velocity to discharge (Leopold and Maddock, 1953).

Flow velocity calculation is a required component of a process-based soil erosion model, and its use requires information about hydraulic roughness. In fact, the hydraulic roughness is a key variable controlling the velocity and the erosivity of the rill flow.

The interaction between flow velocity and changing geometry of a mobile bed rill affects flow resistance.

Many studies have been carried out to understand these erosive forms, several relationships that describe rill hydraulics have been proposed and many equations derived from literature on alluvial rivers have been applied (Foster et al., 1984; Line and Meyer, 1988; Gilley et al., 1990; Govers, 1992; Abrahams et al., 1996; Takken et al., 1998; Hessel et al., 2003; Govers et al., 2007).

The study of the physical processes and mechanisms which determine water erosion becomes a fundamental tool to understand in a better way the problem, estimate the soil loss and try to manage it. To investigate water erosion both empirical and process-oriented models are used.

The most known empirical approach to study the water erosion is the Universal Soil Loss Equation (USLE) (Wischmeier and Smith, 1960) which is composed of six factors (rainfall erosivity R, soil erodibility K, topographic factors L and S, cropping factor C, and management factor P) to predict the long-term (20-25 years) average annual soil loss. Although at first the USLE was developed for erosion plots, then it was integrated to calculate the watershed sediment yield using an operator, as the sediment delivery rate (SDR_w), which takes into account the efficiency in the sediment transport (Williams and Berndt, 1972).

Instead, process-oriented models, as WEPP (Water Erosion Prediction Project, Nearing et al., 1989) try to simulate hydrological and erosive processes at event scale and for different spatial application scales. These models describe erosion sub-processes using hydraulic and hydrology equations, regarding surface flows, soils, and sediment transport.

The rill erosion strictly depends on hydraulic characteristics of the flow which moves within the rill (Foster et al., 1984). The discharge, which characterizes the rill flow, is influenced by the hillslope surface characteristics (roughness, irregularities, obstacles, etc.) and tends to vary along the rill or among the different branches of a rill (main channel and tributaries). To study and model rill erosion processes, in addition to flow discharge, other hydraulic characteristics, as width w, water depth h, mean flow velocity V, and roughness coefficient, must be defined (Gilley et al., 1990).

In particular, the estimate of the mean flow velocity V, can be a huge advantage to apply some soil erosion models, which require its knowledge. This estimate can be obtained applying the two following different approaches based on:

1. hydraulic geometry (Leopold and Maddock, 1953);
2. flow resistance law.

Some Authors have carried out experimental investigations on fixed (Foster et al., 1984; Abrahams et al., 1996) and mobile bed rills (Govers, 1992; Nearing et al., 1997; Takken et al., 1998) (Figure 5) using both the approaches to study and better understand rill hydraulics.

Figure 5. Experimental investigations carried out on rill hydraulics.

Using the first approach, the mean flow velocity can be calculated by the following power equation of the discharge Q:

$$V = kQ^m \quad (1)$$

in which k and m are two coefficients to be experimentally determined. The measurements carried out by Govers (1992) (k = 3.52, m = 0.294), Abrahams et al. (1996) (k = 2.22, m = 0.334) and Govers et al. (2000) (k = 4.19, m = 0.344) highlighted that the coefficient m tends to assume a value close to 0.3. The discrepancies in results of the k coefficient obtained by these Authors are due to the different conditions of bed roughness. In fact, the experiments were carried out on bare soil (Govers, 1992), soil with rock fragments (Govers et al., 2000) and soil covered with gravel elements (Abrahams et al., 1996).

Foster et al. (1984) carried out a laboratory investigation using three fixed bed rills with mean slope s value equal to 3%, 6% and 9%. These Authors obtained a dependence of the mean flow velocity V (m s^{-1}) by the flow discharge Q (m^3 s^{-1}) and the slope expressed by the following equation:

$$V = k_0 Q^{m_0} s^{s_0} \quad (2)$$

in which k_0 = 16, m_0 = 0.28 and s_0 = 0.48.

Di Stefano et al. (2013), using the experimental data of the rills shaped in plots of the experimental area of Sparacia during nine erosive events, tested the applicability of Eq. (2). Rill geometry was analyzed at the end of the event, and being the final result of the morphological evolution, the rill can be considered as a fixed bed channel. In this condition a dependence between the mean flow velocity and the slope should be expected. Di Stefano et al. (2013), obtained the following relationship:

$$V = 8.5Q^{0.26}s^{0.37} \quad (3)$$

Govers (1992), investigating 409 measurements carried out by different Authors on mobile bed rills, found the following empirical equation:

$$V = 3.52Q^{0.294} \quad (4)$$

The approach based on hydraulic geometry does not guarantee an universal estimate of the flow velocity because strictly depends on the site characteristics as the bed roughness. For this reason, an alternative approach has been developed.

The flow resistance law expresses a relationship between the hydraulic characteristics and the friction coefficient as the Darcy-Weisbach friction factor *f* or the Manning's *n*. Since discharge or velocity measurements are not generally available, the general approach has been to apply an empirical flow resistance equation such as Chezy's, Manning's, and Darcy–Weisbach's to substitute for this lack of knowledge (Ferro, 1999; Powell, 2014).

The main problems studying rill flow resistance are that a theory regarding rill hydraulic has not been developed and that hydraulic conditions in rills are very different from those found in large open channel flows (Nearing et al., 1997). In fact, rills geometry evolves rapidly and since the flow is characterized by low water depths, hydraulic characteristics of the flow are influenced by the bed channel morphology (Di Stefano et al., 2017b). Furthermore, rills are characterized by irregular boundaries (Peng et al., 2015). On the contrary, open channel flows are characterized by water depth much higher than the roughness representative size and the morphological evolution is slower than rills.

Notwithstanding the difference between rills and rivers, classical hydraulic equations, such as Manning's and Chezy's equation, are often used in physically based models (Ferro, 1999; Govers et al., 2007; Powell, 2014; Strohmeier et al., 2014; Nouwakpo et al., 2016).

The Chezy's equation, expressed in the Manning's or Darcy-Weisbach's form, assumes the following shape:

$$V = C\sqrt{R\,s} = \frac{s^{1/2}\,R^{2/3}}{n} = \sqrt{\frac{8\,g\,R\,s}{f}} \quad (5)$$

in which C ($m^{1/2}$ s^{-1}) is the Chezy coefficient, R (m) is hydraulic radius and g (m s^{-2}) is acceleration due to gravity.

In most erosion models (EUROSEM (Morgan et al., 1998), GUEST (Hairsine and Rose, 1992a, 1992b), LISEM (De Roo et al., 1996a, 1996b), and CREAMS (Knisel, 1980; Foster et al., 1981)) Manning's equation is applied while the Darcy-Weisbach friction factor is applied in WEPP (Water Erosion Prediction Project) (Foster et al., 1995; Govers et al., 2007; Ferro and Nicosia, 2020).

Govers et al. (2007) stated that rill experiments are useful since <<*provide an opportunity to investigate to what extent the concepts used in models are a truly valid description of the erosion processes occurring*>>. In other words, accurate and repeatable measurements of rill erosion are required to understand the processes and develop a correct rill erosion model (Wirtz et al., 2010; 2012).

Foster et al. (1984) carried out a laboratory investigation using a full-scale fiberglass, fixed bed, replica of a rill. The actual rill was formed during simulated rainfall at 64 mm h^{-1} on a 3.7 m wide by 10.7 m long erosion plot of Russell silt loam soil on a 6% slope. The 0.91 m wide by 4.27 m long replica, which reproduced roughness as small as sand grains, was made from a reach of a rill on the erosion plot. The replica was obtained using a plaster cast and placing the fiberglass over it. In these experiments, the Reynolds number $Re = Vh/\nu_k$, in which ν_k is the water kinematic viscosity, varied from 5700 to 24700. Foster et al. (1984) found that the Darcy-Weisbach friction factor decreases for increasing Reynolds number and justified this behavior with the relationship between the discharge and the bed roughness. Moreover, the relationship between the Darcy-Weisbach friction factor and the Reynolds number is slope independent for $s \geq 6\%$. Foster et al. (1984) established that V increases with a power 0.48 (Eq. 2) of the slope gradient which confirms the applicability of Eq. (5) with a constant f value.

Gilley et al. (1990) carried out experimental runs in 11 US sites on rills under simulated rainfall with slope values between 3.8% and 9.8%. A rainfall intensity equal to 57 mm h^{-1} was used and different inflow discharges (3.16×10^{-4}, 7.57×10^{-4}, 13.3×10^{-4} and 18.9×10^{-4} $m^3 s^{-1}$) were added. The experiments were characterized by Re values from 300 to 10000 (both laminar and turbulent flow regime), and the results confirmed the findings by Foster et al. (1984). In particular, Gilley et al. (1990) obtained the following relationship:

$$f = aRe^{-b} \quad (6)$$

in which the mean values of a and b were equal to 1350 and 0.934, respectively. However, among the different sites, the range of a and b were quite wide ($114 \leq a \leq 527000$ and $0.621 \leq b \leq 1.85$), and this result can be due to the variability of slope values.

Govers (1992) carried out an investigation using four laboratory and field literature databases. This Author observed that, in contrast with fixed bed rills, in mobile bed rills, which are shaped by the channelized flow, mean flow velocity is independent of rill slope s. These findings were confirmed by many Authors as Nearing et al. (1997, 1999), Takken et al. (1998), Hessel et al. (2003) and Giménez and Govers (2001). Assuming as correct the slope independence hypothesis of flow velocity, the use of a constant friction factor in Eq. (5) could be inappropriate for eroding rills. In fact, Eq. (5) allows to obtain a slope-independent rill flow velocity only if the value of Manning's n (Hessel et al., 2003) or the Darcy-Weisbach friction factor f increases with slope gradient.

The hypothesis suggested by Govers (1992) was contradicted by Abrahams et al. (1996). These Authors conducted seventy field experiments in seven rills located on a semiarid rangeland hillslope underlain by gravelly soils at Walnut Gulch, Arizona. Each rill reach was about 3 m long and contained a 0.5 m long test section located about 15 m from the upper end of the reach. Within each test section, three cross-sections were established 0.25 m apart. To prevent scouring by the clear water used in the experiments, the surface of each rill was fixed by sprinkling on it a mixture of one part glue and two parts water. This mixture infiltrated to a depth of several millimeters and sealed the ground surface without perceptibly altering its roughness. This methodology was applied assuming that the hydraulics of clear-water flows over fixed bed rills is similar to that of natural sediment-laden flows over the same unfixed bed. Water simulating rill flow was introduced at the upper end of each reach using a pipe with a pressure gauge and a gate valve. These Authors applying a multiple regression analysis found that, in addition to discharge, flow velocity is related to bed roughness and slope.

Nearing et al. (1997) carried out six experiments on two soils and a uniform sand using three experimental methodologies for mobile bed rills with slope values ranging from 5% to 20% and Reynolds number values lower than 6000. The results of this study challenged the assumption, often used in hydrologic and erosion models, that relationships derived for sheet flow or larger channel flow are applicable to actively eroding rills. Velocity did not vary with slope, and Reynolds number was not a consistent predictor of hydraulic friction. This result was due to interactions of slope gradient, flow rate, erosion, and the formation of rill roughness, bed structures, and head cuts. Nearing et al. (1997) also observed that

Reynolds number does not completely explain the variability of the Darcy-Weisbach friction factor and established that the relationship *f-Re* is dependent on rill slope.

Takken et al. (1998) carried out an experimental study using data obtained by three different setups. First dataset was obtained in a 4.25 m long, 0.4 m wide and 0.6 m deep flume filled with a sandy loam soil in which the rills were incised. Four different values of slope (5, 9, 14 and 21%) and different inflow rates were used. The second dataset was obtained following the same procedures but with soil material mixed with stones. The third dataset consisted of measurements obtained in two different field sites interested by rills. The first site had slope varying from 3 to 5%, whereas the second from 26 to 33.5%. Takken et al. (1998) confirmed the hypothesis by Govers (1992) but found that when the flow has insufficient erosion capacity to adjust the rill geometry a slope effect on flow velocity may be detected.

Giménez and Govers (2001) carried out a laboratory study, in which two situations were compared: i) rills which can freely erode a uniform soil layer and ii) rills with a fixed bed geometry. During the experiments, rill discharge and flow velocity were recorded. After each experiment, a detailed topographic survey of the rill bed was carried out using a laser scanner. From these data the main hydraulic variables (mean values of flow depth, wetted perimeter, and hydraulic radius) were estimated. The experiments confirmed that, when the bed is fixed, the flow velocity in rills is clearly slope-dependent whereas on mobile beds it is not. Giménez and Govers (2001) justified this independence with the concept of "feedback mechanism". In fact, the expected increase of flow velocity due to slope gradient is counterbalanced by the effect of the increase of erosion rate with increasing slope. This last effect produces an increase of bed roughness, thereby slowing the flow velocity.

Hessel et al. (2003) carried out a series of field experiments on a 2.5 m × 0.4 m plot, on which flow could find its own path. Water was evenly applied to the top of the plot and discharge, surface velocity, flow width and slope were measured. The results showed that Manning's *n* can be estimated from Reynolds number. The measurements showed that flow velocity did not increase with slope. These Authors explained this lack of increase in velocity with increased roughness, decreased effective slope angle because of the development of vertical head cuts and a shift in energy use. All three hypotheses only apply to situations involving erosion. The trend of Manning's *n* with slope implies that, in soil erosion models using Manning's equation (or Darcy-Weisbach), the value of *n* (or *f*)

should be a function of the slope for erodible soils. For non-erodible soil (as in woodland), no increase in Manning's n with slope was observed.

Govers et al. (2007) made a critical review of the theoretical concepts that are underpinning rill flow and sediment detachment models. An analysis of empirically collected data on rill hydraulics conclusively showed that the empirical Manning equation does not hold for rill flow and should therefore not be used in rill erosion models. These Authors stated that an empirical power law relationship relating velocity to discharges is much better in agreement with the used experimental data, both for soils with and without rock fragments.

Di Stefano et al. (2013) carried out a field investigation trying to characterize the morphology and hydraulics of both rills and ephemeral gullies. In this study the rill hydraulic geometry was modeled by three well known power equations relating the discharge with the mean flow velocity (Eq. 3), with the flow depth and with the width of each channel segment, respectively. The rill measurements showed that the flow velocity was affected by the rill segment slope while the flow depth and width were controlled by the plot slope.

Strohmeier et al. (2014) conducted some experiments in a 1.95 m long, 0.60 m wide and 0.35 m deep flume with a 10% inclination. At the inlet, a water reservoir with a 0.35 m wide rectangular opening was installed to provide a steady state inflow over the crest of the reservoir. Strohmeier et al. (2014) carried out two different types of experiments: Free Developed Rill (FDR) experiments of unconstrained rill erosion on a plain soil bed and Straight Constrained Rill (SCR) experiments of concentrated flow erosion in a prepared straight initial rill. Each rill experiment (FDR and SCR) was executed with two different discharges (Q_1 = 0.145 L s^{-1} and Q_2 = 0.270 L s^{-1}). The aim of this study was to evaluate the effect of rill morphology on roughness and hence to assess the Manning–Strickler roughness coefficient by rill morphological data. These Authors found that rill flow velocities of SCR experiments increased with an increase in discharge but for FDR experiments no clear trend was indicated since the effect of increased discharge was compensated by increased rill roughness. On the contrary, rill roughness of SCR experiments remained nearly constant for the different discharges which indicates that the friction loss of a straight aligned rill might be properly explained by a constant rill roughness for a specific range of discharge.

Other laboratory experiments were carried out by Peng et al. (2015). In this case, four different values of slope (s = 0.11, 0.18, 0.21 and 0.27) and five different discharges (Q =

0.06, 0.10, 0.20, 0.30, and 0.50 L s^{-1}) were used. These Authors confirmed the findings by Nearing et al. (1997). According to Peng et al. (2015) even though a power relationship as Eq. (6) can be used to estimate *f*, the correlation varies with different values of slope. In particular, for slope values lower than 0.18, *f* gradually decreases for increasing Reynolds number. Instead, for $0.21 \leq s \leq 0.27$, *f* increases for increasing *Re*. These results highlighted the key role of the slope in rill roughness determination.

Flow resistance in natural surfaces is constituted by different components:

1. *grain*-resistance, which is due to the shape, the characteristic dimension and the distribution of the elements which determine bed roughness. Consequently, it strictly depends on surface geometric characteristics. The more the bed roughness increases the more the grain resistance is high. The presence of obstacles (vegetation, woody debris, etc.) causes a further increase of flow resistance.
2. *morphological*-resistance, which is due to the presence of bed forms as step-pools. Step-pools (Figure 6) are characterized by a longitudinal profile which looks like a staircase determined by the alternation of a step and a pool. Most of total flow resistance is composed of the so-called *spill* resistance (Leopold et al., 1964), which is due to the falling down flow and the hydraulic jump inside the pool (Comiti et al., 2007). Briefly, hydraulic losses at steps are mainly produced by nappe flow moving over the step crest and turbulence occurring in the downstream pool.
3. resistance due to sediment transport, which is due to particles detachment and transport phenomena that determine the loss of flow momentum caused by the particles hitting each other (Song et al.,1998) or with the bed (Gao and Abrahams, 2004).

The total flow resistance is the result of these components. In particular, since in nature there are no completely smooth surfaces, *grain*-resistance has always to be considered for natural surface. Step-pool bed forms are a common feature in steep and narrow channels (Chin and Wohl, 2005; Curran and Wilcock, 2005; Church and Zimmermann, 2007; Comiti et al., 2005; 2009; Waters and Curran, 2012) and are created by discharge with high rates of sediment influx and transport. Steps may be mobilized by large flows without significant sediment transport (Rosport, 1994). In particular, individual steps within a sequence can shift their position after initial deposition when flows lower than the step-setting flow occur (Waters and Curran, 2012). Not all steps experience a shift in their position (Turowski et al., 2009), and those steps that do not migrate

downstream are eroded more quickly. Step sequence stability is associated with the maintenance of the spacing between steps with time; step sequence stability occurs when the step spacing corresponds to the maximum overall channel flow resistance.

Figure 6. View of a step-pool sequence occurred during an experimental run.

The resistance to flow in step-pools is mainly due to form-induced mechanisms and, in comparison, grain resistance is of minor significance (Canovaro et al., 2004; Church and Zimmermann, 2007; D'Agostino and Michelini, 2015). Classical resistance formulations based on the dominance of grain resistance should not successfully describe the resistance to flow in step-pools (Aberle and Smart, 2008; Church and Zimmermann, 2007). Giménez and Govers (2001) tried to explain the bed geometry–flow hydraulics feedback in step-pool rills hypothesizing a mechanism, constituted by the following steps:

1. small local variations in flow depth, velocity, and soil erodibility produce local erosion and the formation of a small depression in the bed;

2. this depression causes a hydraulic jump, and its energy dissipation produces additional local erosion and a pool is formed;
3. within the pool, the flow is subcritical;
4. the flow accelerates in the downstream direction to become supercritical;
5. a succession of pools in which the flow is subcritical and steps with supercritical flow occurs.

This hypothesis has been positively tested by flume measurements carried out by Giménez et al., (2007), which showed that across steps rill flow is rapidly accelerating until a Froude number ($F = V/\sqrt{gh}$), varying from 1.3 to 1.7, is reached. The hydraulic jump downstream the step, determines the formation of a pool and the subcritical flow leaving the pool, which accelerates over the next step.

Finally, resistance due to sediment transport occurs only for mobile bed rills or fixed bed rills with a sediment-laden flow. Consequently, for experiments carried out on a fixed bed and with clear flow this type of resistance does not occur. Two different types of sediment transport can be distinguished: *a) bed-load transport*, which consists in saltation, rolling and drag on the bed surface of heavier sediments; *b*) *suspended load*, which consists in the transport by the flow of finer particles in suspension.

Many authors (Baiamonte and Ferro, 1997; Campbell et al., 2005; Chow, 1959; Ferro, 2018a; Gao and Abrahams, 2004; Recking et al., 2008; Song et al., 1998; Vanoni and Nomicos, 1960; Wang et al., 2011), studying sediment transport, concluded that flow resistance increases when sediments are added to a clear water flow. In particular, Recking et al. (2008) confirmed that flow resistance increases for increasing sediment amount until the sediment rate G is equal to the flow transport capacity T_c. These Authors also found that if this sediment transport equilibrium condition ($G = T_c$) occurs, the Darcy-Weisbach friction factor f increases with sediment concentration.

Vanoni and Nomicos (1960), studying the effect of bed-load movement on friction factor, suggested that flow resistance is much more affected by variations in bed configurations than those due to the suspended load.

Jiang et al. (2018), studying the sediment transport capacity, carried out an experimental investigation by a rill flume, 0.12 m wide and 4 m long. The used hydraulic scheme simulates a rill having a rectangular cross-section with fixed smooth sides and a no-erodible rough bed in which the flow has a *sediment load* equal to the transport capacity T_c. The 35 experimental runs were carried out by a colluvial soil (3% clay, 32.8% silt and 64.2% sand) for seven slope steepness (s = 18, 27, 36, 47, 58, 70 and 84%) and five

different discharges ranging from 0.0672 to 0.528 L s^{-1}. The experimental runs were carried out for hydraulic conditions characterized by Reynolds number of $639 < Re < 5529$ and Froude number ranging from 1.57 to 8.14.

Rill erosion processes need to be monitored and quantified. A better knowledge of the processes can be achieved by surveying these erosive forms for measuring the amount of soil detached and deposited within rills.

Rill erosion measurements can be made by traditional direct field methods or applying indirect techniques (*image-based* and *laser scanner*). The direct method implies measurement of rill erosion based on the assessment of some cross-section areas along the rill channel. The direct method is very simple, low-cost, time-consuming, and widely used (Casalì et al., 2006). Rill cross sections can be measured using a pin profiler (rillmeter), which consists of some stainless-steel pins having a transverse constant spacing, which is placed perpendicularly to the channel axis (Bruno et al., 2008) (Figure 7). Characterization of a cross section by a tape and a ruler requires that each cross section be assimilated to a simple geometric form. Tape is usually used for direct measurement of field horizontal distance, while a ruler is used for measuring the water depth values. The measurements at plot scale by the traditional direct method (i.e., metric ruler, rillmeter, topographic instruments) are limited by the fact that the surface of the rilled area tends to be modified.

Figure 7. View of a rillmeter (Di Stefano et al., 2019a).

Instead, ground measurement of rill features using indirect methods is considered a non-invasive method allowing a fast field survey.

Indirect methods are generally based on use of Terrestrial Laser Scanning (TLS) (Vinci et al., 2015) or *image-based* techniques (Carollo et al., 2015; Di Stefano et al. 2017b; 2017c), which are cheaper than TLS and allow to obtain 3D models as much accurate and precise. Close-range photogrammetry can be effectively used to measure soil erosion processes using recent advancements in automatic 3D-photo reconstruction (3D-PR) techniques. These techniques use oblique images acquired from uncalibrated and non-metric cameras coupled with photogrammetric software packages (Castillo et al., 2012). Terrestrial digital photogrammetry has a little impact on ground measurements, is a technique characterized by high spatial resolution (centimeters to millimeters) and it requires a time-consuming work for post-processing the digital photos acquired in the field activity. Image-based modeling creates a digital terrain model (DTM) using a set of oblique photographs taken from the same rilled surface (Frankl et al., 2015) and without using control points during the composition of the model (Gómez-Gutiérrez et al., 2014). Camera model parameters and scene geometry are simultaneously solved (James and Robson, 2012), using redundant information coming from oblique photographs. The generated point cloud has to be scaled and georeferenced using some ground control points located within the monitored rilled area. Main advantages of 3D-PR method are both that it requires little expertise because the image processing is almost automatic (James and Robson, 2012), and that it has a high accuracy. Semi-automated 3D-PR techniques, such as the coupled use of Structure from Motion (SfM) and MultiView-Stereo (MVS) workflows (Javernick et al., 2014, Seiz et al., 2006), are integrated in software packages such as Photoscan (Agisoft) (Frankl et al., 2015).

Measuring rill erosion by an image-based technique requires the use of a 3D Digital Terrain Model (3D-DTM) model which can represent the three-dimensional topography also including areas into which different z-elevations can be associated to the same couple of plane coordinates x-y. On the contrary, the 2.5D model (Digital Elevation Model, DEM) represents the surface of the rilled area by a vertical perspective; in other words, 2.5D model cannot represent cross-sections having undercut walls (Frankl et al., 2015) in which the coordinates x–y of a ground measurement point can correspond to different z elevations. In this case, the 2.5D model underestimates the area of the cross-section and, as a consequence, the eroded rill volume (Di Stefano et al., 2017b) (Figure 8). However, the 2.5D model is often used for hydrological analyses and it can be easily managed being a raster model.

Di Stefano et al. (2017b) assessed the applicability of the SfM technique using the measurements obtained for three small channels. These Authors compared the measurements obtained by 3D, 2.5D and profilometer. The comparison between the real channel volumes, measured filling the channels with a known water amount, and those obtained by the application of the models showed excellent results. In particular, the volume estimated using the 3D model gave errors less than 0.5%.

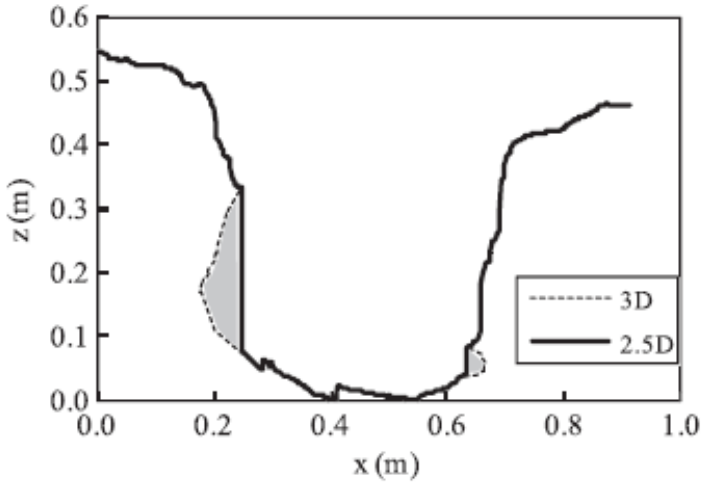

Figure 8. Comparison between the profiles obtained by 3D and 2.5D models (grey indicates the areas that 2.5D model is not able to represent) (Di Stefano et al., 2017b).

Di Stefano et al. (2017c) also applied SfM-technique for rill channels shaped in a plot. This investigation was carried out creating a rill network composed by two main rills (6.24 m long) and five tributary reaches. In particular, to test the accuracy of 3D model, a 6m long gypsum cast was realized for one rill. The comparison between the measurements (surface width, maximum depth, cross-section area, perimeter, and hydraulic radius) obtained by the gypsum cast in 11 cross-sections and those obtained by 3D model confirmed the reliability of the 3D model. Furthermore, Di Stefano et al. (2017c) realized other three rills in an experimental plot for testing the shaping effect of the flow discharge. The experimental runs were carried out using different inflow discharges, until the storage tank at the outlet of the plot was filled with 308 L of the suspension (liquid + solid fractions). This suspension was collected and then oven dried at 105 C° to obtain the sediment weight. The difference between the 3D model of the initial condition and that of the final one allowed to calculate the volume of soil eroded by a known inflow discharge. This volume was converted into weight using the bulk density. The comparison between the real

soil loss amount and that obtained by the 3D model confirmed the reliability of the 3D model for measuring rill erosion.

Other Authors (Stöcker et al., 2015; Glendell et al., 2017) positively tested the use of GP (ground-based photogrammetry) and UAV (*Unmanned aerial vehicles*) based photogrammetry on some gullies.

Ground-based photogrammetry is useful to study areas with extension between 10 and 100 m (James and Robson, 2012; Smith, 2014), while UAV are more adequate for wider areas.

In conclusion, the applicability of SfM-technique was widely assessed using different surveys (GP and UAV) at different scales (rill, ephemeral-gully and gully).

Ferro (2017) deduced a new resistance law for open channel flow applying dimensional analysis and self-similarity theory. The incomplete self-similarity hypothesis was used to establish the flow velocity distribution whose integration gives the theoretical expression of the Darcy-Weisbach friction factor. This theoretical resistance equation was tested by the available field measurements of flow velocity, water depth, river width and bed slope carried out in 653 reaches of several Canadian mountain streams. Ferro (2018b) and Ferro and Porto (2018) assessed this approach using 416 flume experimental runs with gravel bed and 104 reaches of Calabrian gravel-bed rivers (*fiumare*), respectively. This approach was also successfully tested for overland flows in different conditions as: smooth bed under simulated rainfall (Nicosia et al., 2020a) using the literature data by Yoon and Wenzel (1971); rough bed on a stony hillslope under simulated rainfall (Nicosia et al., 2020b) using the data by Nearing et al. (2017); rough bed with presence of vegetation under simulated rainfall (Nicosia et al., 2020c) using the data published by Polyakov et al. (2018).

1.3. *PhD thesis purpose*

The aim of this Ph.D. dissertation is the application of the forementioned theoretical expression of the Darcy-Weisbach friction factor using measurements obtained for rills at plot scale. In particular, the experiments were carried out on different soils, characterized by different slopes, for both mobile and fixed bed rills. The measurements allowed to calibrate the flow resistance equation for the different tested conditions and investigate the contribution of both *grain*-resistance and resistance due to sediment transport to the total flow resistance. Since during some runs step-pool features occurred, the *morphological*-resistance was also studied. In detail, in this Ph.D. dissertation the following objectives were pursued: *a*) to investigate the effects of *grain*-resistance and soil texture on total flow

resistance; *b*) to study the differences determined by the occurrence of step-pool units and the consequent *morphological*-resistance; *c*) to compare the behavior of flow resistance in mobile and fixed bed rills; *d*) to determine the contribution to the total resistance due to sediment transport phenomena, and *e*) to test the slope independence hypothesis of flow velocity for mobile and fixed bed rills.

2. THE THEORETICAL FLOW RESISTANCE EQUATION

For an open channel flow the discharge can be calculated if a theoretical distribution can be applied to the velocity profiles measured in different verticals of the cross section (Ferro and Baiamonte, 1994), and the relationships that establish how the coefficients of the theoretical distribution (logarithmic, power, Dean–Finley; Baiamonte et al., 1995; Ferro, 2003) vary from one vertical to another can be determined (Ferro and Giordano, 1993).

Flow resistance law was theoretically deduced for those sections characterized by simmetry (circle, infinitely wide rectangular) and well-known boundary conditions, for which the velocity distribution law could be deduced. For the forementioned sections, the Prandtl-von Karman theory, for turbulent flow regime, allows to deduce the logarithmic law of the velocity distribution (Ferro, 2003). Integrating the velocity distribution, the mean flow velocity V can be determined and, consequently, the following flow resistance law for turbulent flow regime and micro-roughness conditions, can be defined:

$$\sqrt{\frac{8}{f}} = A + B \log\left(\frac{R}{d}\right) \tag{7}$$

in which A and B are two coefficients and d depends on the absolute roughness.

Considering that the flow resistance law can be expressed by a functional relationship representing the examined physical process, the dimensional analysis can be usefully employed (Barenblatt, 1993; Ferro, 1997).

According to the Buckingham's theorem of the dimensional analysis (Barenblatt, 1979; 1987), the functional relationship, representing a physical phenomenon that is independent of the used measurement units for the involved variables, can be expressed in a dimensionless form. Using dimensionless groups permits testing of the global effects of the variables that occur in each group rather than the effect of each single variable (Ferro, 1997).

A phenomenon is defined self-similar in a given Π_n dimensionless group when the functional relationship $\Pi_1 = \phi(\Pi_2, \Pi_3, \ldots\ldots, \Pi_n)$ representing the physical phenomenon is

independent of Π_n. The self-similarity solutions of a problem are searched for boundary conditions, that is, the behavior of the function ϕ is studied for $\Pi_n \to 0$ and $\Pi_n \to \infty$. When the function ϕ tends to a finite limit and this limit is different from zero, the phenomenon is not influenced by Π_n and is expressed by the functional relationship $\Pi_1 = \phi_1(\Pi_2, \Pi_3, \ldots\ldots, \Pi_{n-1})$, in which ϕ_1 is a functional symbol, and the self-similarity is named complete self-similarity (CSS) in a given Π_n dimensionless group.

When the function ϕ has a finite limit equal to zero or tends to infinity, the phenomenon is expressed by the following functional relationship:

$$\Pi_1 = \Pi_n^{\beta} \phi_2\left(\Pi_2, \Pi_{3,\ldots\ldots\ldots,} \Pi_{n-1}\right) \tag{8}$$

in which $\phi 2$ is a functional symbol and β is a numerical constant. This instance is named incomplete self-similarity (ISS) in the parameter Π_n (Barenblatt, 1979, 1987).

Barenblatt (1993) emphasized that the derivation of the universal logarithmic distribution and the power-type law used for representing the local mean velocity distribution $v(y)$, in which v is local velocity and y is distance from the bottom, is equally rigorous even if it is based on entirely different basic assumptions.

For a uniform turbulent flow in an open channel, the flow velocity distribution along a given vertical can be expressed by the following functional relationship (Barenblatt, 1987, 1993; Ferro, 1997):

$$\phi\left(\frac{dv}{dy}, y, h, d, u_*, \rho, \mu\right) = 0 \tag{9}$$

in which d is the roughness height, $u_* = \sqrt{gRs}$ is the shear velocity, ρ is the water density and μ is the water dynamic viscosity.

According to the Π-theorem (Barenblatt, 1987), Eq. (9) can be expressed in a dimensionless form as follows:

$$\Pi_1 = \phi_3\left(\Pi_2, \Pi_{3,} \Pi_4\right) \tag{10}$$

where Π_1, Π_2, Π_3 and Π_4 are dimensionless groups and ϕ_3 is a functional symbol.

Using as dimensionally independent variables y, u_*, and μ, the following expression of the dimensionless group Π_1 can be obtained:

$$\Pi_1 = \frac{dv}{dy} y^a u_*^b \mu^c \tag{11}$$

where a, b and c are numeric values. Substituting into Eq. (11) the corresponding unit of measurement for each variable, the following equation is obtained:

$$\Pi_1 = LT^{-1}L^{-1}L^a L^b T^{-b} F^c T^c L^{-2c} \tag{12}$$

in which L is length, T is time and F is force.

Since the group Π_1 is dimensionless, a, b and c can be deduced solving the system of three equations which is obtained by Eq. (12):

$$0 = 1 - 1 + a + b - 2c \tag{13a}$$

$$0 = -1 - b + c \tag{13b}$$

$$0 = c \tag{13c}$$

Introducing the values obtained solving the system of Eq. (13) into Eq. (11) the group Π_1 can be represented by the following relationship:

$$\Pi_1 = \frac{y}{u_*}\frac{dv}{dy} \tag{14}$$

Applying this procedure to each dimensionless group the following relationships representing Π_2, Π_3 and Π_4 were obtained:

$$\Pi_2 = \frac{h}{y} \tag{15}$$

$$\Pi_3 = \frac{d}{y} \tag{16}$$

$$\Pi_4 = \frac{u_* y}{\nu_k} \tag{17}$$

Furthermore, according to Barenblatt (1987), "In some cases, it turns out to be convenient to choose new similarity parameters—products of powers of the similarity parameters obtained in the previous step." In other words, Barenblatt (1987) suggested combining the original dimensionless groups to obtain new similarity parameters.

From Eqs. (15) and (16) it follows:

$$\Pi_{2,3} = \frac{\Pi_2}{\Pi_3} = \frac{h}{y}\frac{y}{d} = \frac{h}{d} \tag{18}$$

Coupling Eqs. (17), (16), and (15), the following dimensionless group is obtained:

$$\Pi_{4,3,2} = \Pi_4\Pi_3\Pi_{2,3} = \frac{u_* y}{\nu_k}\frac{d}{y}\frac{h}{d} = \frac{u_* h}{\nu_k} \tag{19}$$

The functional relationship (10) can be rewritten in the following form:

$$\Pi_1 = \phi_4(\Pi_4, \Pi_{4,3,2}, \Pi_{2,3}) \tag{20}$$

in which ϕ_4 is a functional symbol.

Introducing into Eq. (20) the Eqs. (17), (18) and (19), the functional relationship can be rewritten as follows:

$$\frac{y}{u_*}\frac{dv}{dy} = \phi_4\left(\frac{u_* y}{\nu_k}, \frac{u_* h}{\nu_k}, \frac{h}{d}\right) \tag{21}$$

If the CSS hypothesis in u_*y/ν_k, u_*h/ν_k, and h/d is assumed, the Π group is constant, and by integrating Eq. (9), the logarithmic law is obtained. In other words, the hypothesis of CSS

in u_*y/ν_k, u_*h/ν_k, and h/d is equivalent to assuming a constant value of the von-Karman constant K. The dependence of K on flow Reynolds number, pointed out by Tennekes (1968) (Ferro and Pecoraro, 2000), limits the validity of the CSS hypothesis, which is the basis of the logarithmic law.

According to the theory of self-similarity (Barenblatt, 1987), if the experimental results do not permit to hypothesize a CSS, an ISS solution of the problem has to be found (Barenblatt and Monin, 1979). Assuming the ISS in u_*y/ν_k, the following power velocity distribution is obtained (Ferro and Pecoraro, 2000):

$$\frac{V}{u_*} = \Gamma\left(\frac{u_* y}{\nu_k}\right)^{\delta} + C_1 \tag{22}$$

in which Γ is a function to be defined by velocity measurements and C is an integration constant, which can be assumed equal to zero (Barenblatt and Prostokishin, 1993; Ferro and Pecoraro, 2000).

Barenblatt (1991), on the basis of the studies of Castaing et al. (1990) and some results of the geometry of dissipative vortex structures, suggested the following theoretical equation for the δ exponent:

$$\delta = \frac{1.5}{\ln Re} \tag{23}$$

Integrating the power velocity distribution (Eq. 22), with $C = 0$, Barenblatt (1993) deduced the following expression of the Darcy–Weisbach friction factor f:

$$f = 8\left[\frac{2^{1-\delta}\,\Gamma\; Re^{\delta}}{(\delta+1)\,(\delta+2)}\right]^{-2/(1+\delta)} \tag{24}$$

Taking into account that $(f/8)^{1/2} = Re_*/Re$, in which $Re_* = u_*\, d/\nu_k$ is the shear Reynolds number, from Eq. (24), the following expression of Γ is obtained:

$$\Gamma_v = \frac{(\delta+1)(\delta+2)Re}{2^{1-\delta}Re_*^{1+\delta}} \tag{25}$$

Setting into Eq. (22), with $C = 0$, $y = \alpha\, h$ the distance from the bottom at which the local velocity is equal to the mean value V, it follows:

$$\Gamma_v = \frac{V}{u_*\left(\frac{u_*\,\alpha\, h}{\nu_k}\right)^{\delta}} \tag{26}$$

in which the coefficient α, less than 1, takes into account that both the velocity V is located below the water surface and a single velocity profile in the cross section is considered.

Equalizing Eq. (25) and Eq. (26) results in:

$$\frac{(\delta+1)(\delta+2)}{2^{1-\delta}}\frac{Re}{Re_*}\frac{1}{Re_*^{\delta}} = \frac{Re}{Re_*}\frac{1}{\alpha^{\delta}Re_*^{\delta}} \tag{27}$$

from which the following equation for calculating α is deduced:

$$\alpha = \left(\frac{2^{1-\delta}}{(\delta+1)(\delta+2)}\right)^{\frac{1}{\delta}} \quad (28)$$

Di Stefano et al. (2017a), for 2,000 ≤ *Re* ≤ 10,000, which is usually the measurement range in rill flows, coupling Eqs. (28) and (23), obtained a very narrow range of the calculated α values and a mean of 0.124 which could be considered the representative value of α. Therefore, from Eq. (26), the following estimate Γ_v of Γ function is obtained:

$$\Gamma_v = \frac{V}{u_* \left(\frac{u_* \, 0.124 \, h}{\nu_k}\right)^{\frac{1.5}{lnRe}}} \quad (29)$$

Ferro (2018b) demonstrated that, since *F* takes into account both the depth sediment ratio *h/d*, and the shear Reynolds number Re_*, Γ_v is only dependent on channel slope and flow Froude number. In particular, the relationship between Γ_v, *F* and *s* is expressed by the following power equation:

$$\Gamma_v = \frac{a \, F^b}{s^c} \quad (30)$$

in which *a*, *b* and *c* are coefficients which have to be estimated by the available experimental data.

3. MATERIALS AND METHODS

3.1. *Experimental plots, set-up, and procedures*

The experiments were carried out on rills shaped on two plots (Figure 9), located at the experimental area of the Department of Agriculture, Food and Forest Sciences of the University of Palermo. Each plot, 2 m wide and 7 m long, has a base built by gabions and is bounded by concrete walls. At the plot downstream end is located a storage tank, having the same width of the plot and a cross-section 0.7 m wide and 0.4 m high. On the plot boundaries some targets (two at the top vertices, two at the bottom vertices and two at the middle of the plot) were fixed and then detected by a total station to be used as Ground Control Points (GCPs) within the procedure of 3D photo-reconstruction of the plot surface. The rills were manually incised excavating a small channel along the plot maximum slope direction and further enlarged and deepened by introducing at the inlet section a shaping clear flow discharge (0.1 L s^{-1} applied for 3 minutes). Water simulating rill flow was introduced at the upper end of each tested rill by a small pipe.

Figure 9. View of the experimental plots.

A constant inflow clear discharge Q from the pipe was directed towards the rill by an inflow device (Figure 10), with wire meshes, useful to dissipate flow turbulence. The discharge values were measured by the volumetric method measuring the filling time of a plastic bucket of known volume with a chronometer. In the first shaping phase (discharge 0.1 L s^{-1}), the "bulldozer effect" (Regüés et al., 2000; Seeger et al., 2004), which is "a mobilization of the loose material available in the rill before an experiment starts" (Wirtz et al., 2012), occurred. In this first phase, the flow discharge and the corresponding transport capacity were low; as a consequence, the rill flow was saturated (the actual *sediment load* was equal to the transport capacity) by the sediment particles available from the "bulldozer effect," and the soil detachment due to rill flow was negligible.

The experiments were carried out using five soils characterized by different textures. In particular, the textural fractions vary from 32.7% to 73% for clay, from 19.9% to 30.9% for silt, and from 4.5% to 36.4% for sand. Different plot slope values s_p, equal to 9, 14, 15,

18, 22, 24, 25 and 26%, were examined. In Table 1 the plot slope values, and the corresponding soil textures are listed.

Figure 10. View of the inflow device.

Figure 11 shows the soil texture distribution on Miller's triangular diagram. Four soils are classified as "clay", while only one is classified as "clay loam" (CL) (yellow point corresponding to s_p= 9 and 15%).

The experimental runs were carried out with two different configurations of the rill bed. Most of the runs were carried out for a mobile bed rill condition, in which the bed could be eroded (detachment and transport phenomena) by the flow. When the constant inflow discharge entered the shaped rill channel, the flow was able to simultaneously transport the loose material available in the mobile bed rill, after the shaping phase, and the detached particles from the rill wetted perimeter.

Table 1. Characteristic data of plot slope values s_p and corresponding soil textures used in this investigation

s_p	*CLAY*	*SILT*	*SAND*
%	%	%	%
9	62	26.4	11.6
9	32.7	30.9	36.4
14	73	22.5	4.5
15	32.7	30.9	36.4
18	62	26.4	11.6
22	62	26.4	11.6
24	42	23.5	34.5
25	71	19.9	9.1
26	71	19.9	9.1

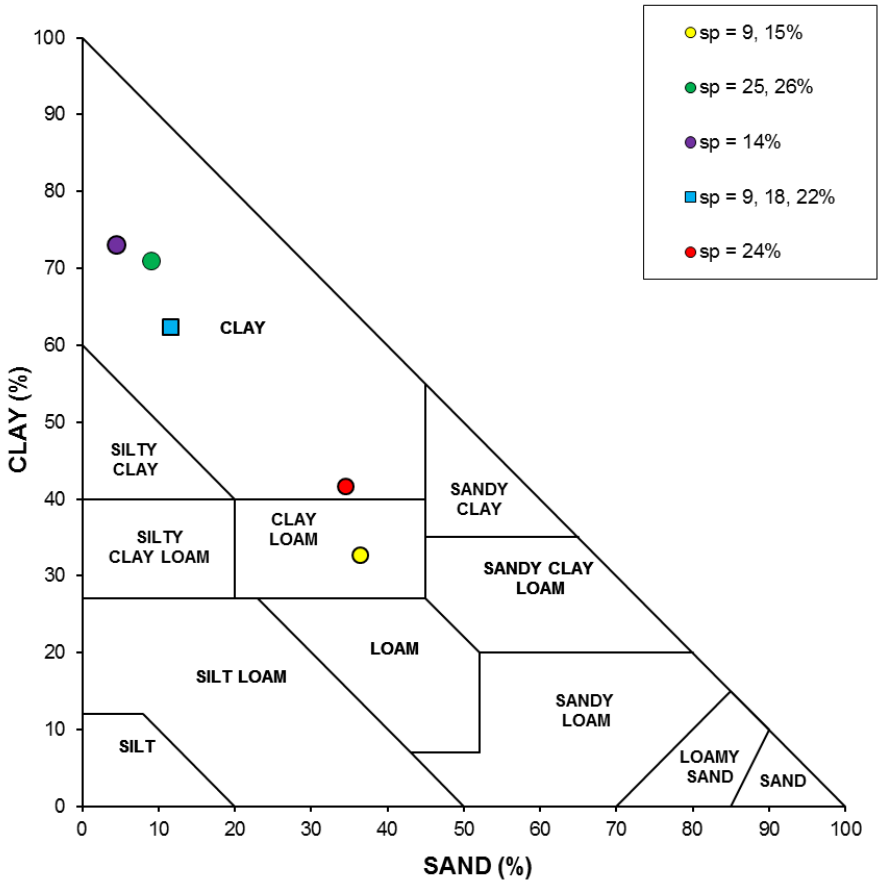

Figure 11. Soil texture distribution on the Miller's triangular diagram.

Figure 12 shows, as an example for s_p = 18%, the spatial distribution of the scouring of the rill channel produced first by the shaping discharge (Figure 12a) and then by the discharge used for the experimental runs (0.29 to 0.87 L s^{-1}) (Figure 12b). The 3D-photo reconstruction technique was applied for obtaining the digital elevation model (DEM) at the end of the rill manual incision (D_0), at the end of the shaping phase (D_1), and at the end of the experimental runs (D_2). The scour depths due to the shaping discharge (0.1 L s^{-1}) was obtained using the DEM of difference between D_1 and D_0 (D_OD_1), whereas those due to the discharge applied in the experimental run (0.29–0.87 L s^{-1}) was obtained using the DEM of difference between D_2 and D_1(D_OD_2). Figure 12 clearly demonstrates that both the shaping phase and the experimental runs produced a deepening of the cross sections.

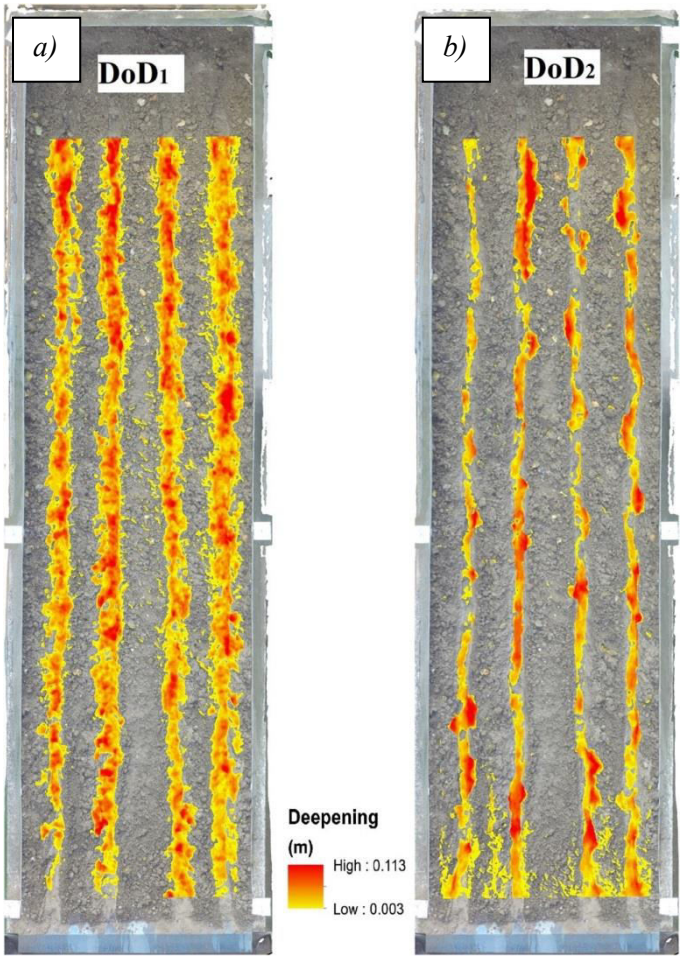

Figure 12. Spatial distribution of the scour depth at the end of both the shaping phase (a) and the experimental run (b).

Other runs were carried out fixing the rill bed. The rill channel perimeter was fixed by sprinkling on it a mixture of waterproof vinylic glue and water (1:2) (Figure 13). Spraying was continued until glue infiltration stopped and after the application, the glue was left to

dry for 24 hours. For fixed bed rills two different conditions were tested: *a)* the runs were carried out at the end of the corresponding mobile bed ones, fixing the surface of each rill channel; *b)* the runs were carried out fixing rills after the shaping phase. For the first condition the experiments were carried out for plot slope values s_p equal to 9 (clay), 22, 24, 25 and 26%, whereas for the second one the slope values s_p were equal to 9 (clay loam) and 15%.

Figure 13. Fixing bed rills with mixture of waterproof vinylic glue and water.

For some runs (corresponding to some discharge values for s_p equal to 14, 22, 24 and 26%) step-pool bed forms occurred during the shaping phase. In this case, the longitudinal rill bed profile showed a sequence of step-pool structures (Figure 14); the form of each step-pool is characterized by a step spacing length L_i measured parallel to the direction corresponding to the average bed slope angle θ (Abrahams et al., 1995). At first, on the longitudinal rill bed profile, the step spacing length was visually established identifying the initial (step) and the final (pool) point in correspondence to an abrupt local slope change. Then, for each investigated rill, the 3D-DTM was used to automatically extract steps using the critical slope method of Milzow et al. (2006), where segments having slope values s_i larger than a critical value are used for defining the starting point of a step.

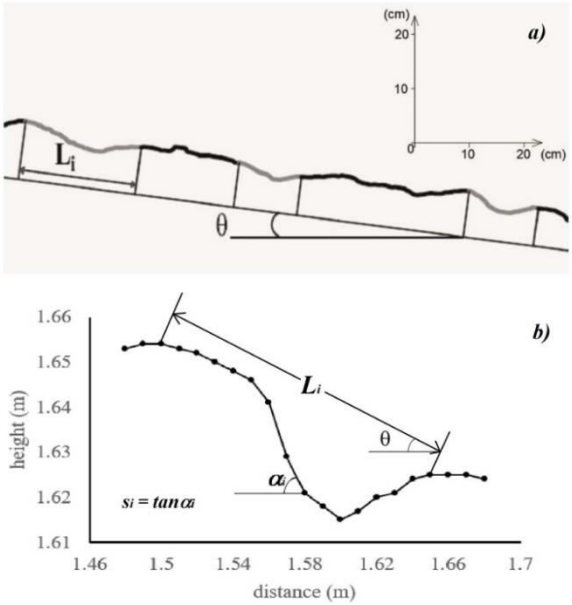

Figure 14. Example of a rill thalweg extracted by a 3D-DTM (a) and definition of the step spacing length L_i (b).

In each rill 10 measurement cross-sections were set with a constant longitudinal distance equal to 0.624 m, determining 9 longitudinal segments bounded by two consecutive cross-sections. A reach was defined as a rill portion between a measurement section and the rill end (Figure 15). Therefore, 9 reaches were established for each rill channel.

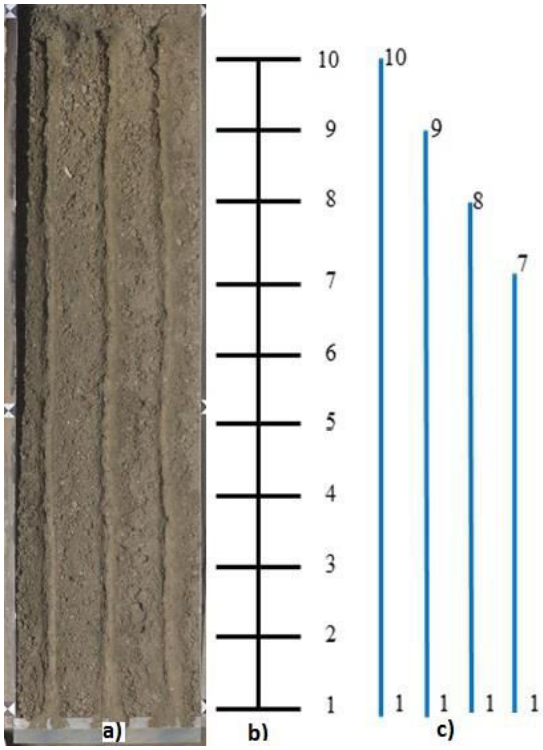

Figure 15. Plan view of the experimental plot (a), scheme of the cross-sections (b), and of the rill reaches (c).

3.2. *Ground measurement technique*

An image-based technique was applied for carrying out the ground measurements of rill cross-section area σ, wetted perimeter *C* and reach slope *s*. In particular, the terrestrial survey was executed using a GoPro Hero4 camera fixed to the tip of a telescopic pole (Figure 16) to capture high centre-perspectives of the plot by following a walking itinerary around the plot.

Figure 16. View of field survey by photographic method.

Image overlapping assured that any point of the measured plot area was represented in at least 3 photographs for taking into account that the SfM algorithm is designed to work with convergent images. For creating the DTM, the image-based modeling technique was applied by a set of about 70 photographs taken from the plot area. The image-processing software Agisoft Photoscan Professional was used for obtaining the 3D model (Figure 17) by an automatic process which couples the SfM and MVS techniques (Frankl et al., 2015; Javernick et al., 2014; Seiz et al., 2006; Di Stefano et al., 2017b).

Figure 17. View of the DTM of the plot area, with some tested rills and six ground control points, and of some cross-sections.

This software includes all the steps for model creation, from the raw data (the photographs) to 3D point cloud, 3D triangulated mesh, 2.5D model and orthophoto with a workflow that is simple and user-friendly. The survey of the plot surface was carried out before and after the experimental runs.

Georeferencing error based on the root mean square error (*RMSE*) of ground control points was used to assess the accuracy of the 3D point clouds. The 3D point clouds were characterized by almost constant values of *RMSE* with a mean of 2 mm. This is a low value compared to the spatial extent of the features of interest.

The resolution of the 3D-DTM was set equal to the mean ground sample distance, *GSD*, which is the actual terrain surface represented into the pixel of the camera sensor and is calculated as $\sigma_{pix}H/f_d$, where σ_{pix} is the pixel size, H is the average object distance and f_d is the focal length. The detail level of the 3D model increases as *GSD* decreases.

For the camera used in this investigation, σ_{pix} was equal to 0.00173 mm and f_d was equal to 3 mm. Using a mean value of H, representative of the different terrain surveys, equal to 1.8 m, a corresponding *GSD* value equal to 1.04 mm was obtained.

3.3. *Hydraulic measurements*

The used inflow discharge values ranged from 0.1 to 1 L s^{-1}. The flow velocity was measured using the dye tracing method (Abrahams et al., 1996; Govers, 1992; Line and Meyer, 1988; Di Stefano et al., 2018a, 2018b, 2020). A Methylene blue solution was used as a dye injecting a small amount (3 mL) in the measurement cross-section with a Pasteur pipette. The surface flow velocity V_s was then measured by recording the travel time of the leading edge of the dye cloud over the reach length (Figure 18).

Figure 18. Flow velocity measurement by the dye tracing method using a Methylene blue solution.

A correction factor α_v has been applied to convert V_s to the mean flow velocity V (Zhang et al., 2010). Many studies have been carried out to determine the correct value of α_v in dependence of different flow regime and bed roughness. Emmett (1970), carrying out flume experiments, demonstrated that α_v increases with flow Reynolds number and is close to 0.8 for turbulent flow. In flume experiments using a gravel bed, Luk and Merz (1992) obtained a mean value of α_v equal to 0.75 for turbulent flow. Li and Abrahams (1997) carried out a set of experiments to measure α_v for overland flow without sediments on a fixed bed using three slope values. For a sediment-free turbulent flow ($Re \geq 8{,}000$), Li and

Abrahams (1997) established that α_v is independent of slope and assumes a nearly constant value equal to 0.8. For a given *Re* value, α_v decreases for increasing values of the *sediment load* (Zhang et al., 2010). In the light of the results available in literature and considering that the correction factor value has an almost negligible effect on the estimate of the Darcy-Weisbach friction factor (Di Stefano et al., 2018a), a constant α_v value equal to 0.8 was used.

In each run, the water depth values were measured in the 10 test cross-sections by a micro-hydrometer (Figure 19), having a measurement accuracy of ±1 mm. The water depth was equal to the difference between the elevations at the rill thalweg and flow surface. Only one measure of water depth for each cross-section was carried out to avoid a long-lasting run which could have caused a relevant change of the rill geometry.

The cross-section area and wetted perimeter were determined by using the measured water depth in combination with the geometric cross section profile extracted by 3D-DTM related to the final condition of the run.

Figure 19. View of a micro-hydrometer.

The water depth h, the hydraulic radius R and the slope gradient s of each reach were calculated by averaging the values measured in the considered reach. For each reach Froude number F, Reynolds number *Re* and shear velocity u_* were also calculated. The Darcy-Weisbach friction factor f of the reach was indirectly measured by using Eq. (5) with the above measured values of V, R and s.

The measurements were carried out for both subcritical and supercritical flow conditions (F ranging from 0.47 to 3.54) and laminar, transition and turbulent flow regime (Re ranging from 859 to 14495).

In Table 2, for each bed condition and slope value, the ranges of the characteristic data are listed.

Table 2. Ranges of characteristic data, for each bed condition and plot slope value s_p.

s_p	Q	h	s	V	F	Re	f
%	L s^{-1}	m	m m^{-1}	m s^{-1}			
MOBILE BED							
9 (clay)	0.36-0.98	0.010-0.021	0.073-0.131	0.32-0.66	0.89-1.90	3208-8537	0.17-0.57
9 (clay loam)	0.21-0.87	0.015-0.029	0.051-0.115	0.26-0.62	0.60-1.38	3860-12895	0.14-1.17
14	0.36-1.00	0.006-0.023	0.071-0.193	0.23-0.90	0.64-3.03	2169-10723	0.06-1.62
15	0.19-0.87	0.013-0.026	0.094-0.228	0.26-0.63	0.69-1.70	2872-9990	0.14-1.46
18	0.29-0.87	0.011-0.037	0.137-0.239	0.32-0.55	0.70-1.33	3615-14945	0.43-1.67
22	0.35-1.00	0.004-0.017	0.092-0.259	0.26-0.56	0.74-1.76	1306-5539	0.39-1.63
24	0.11-0.86	0.005-0.027	0.125-0.238	0.22-0.69	0.67-1.67	919-9520	0.17-1.92
25	0.25-0.87	0.009-0.020	0.203-0.25	0.29-0.69	0.87-1.95	2505-9588	0.33-1.31
26	0.15-0.52	0.006-0.023	0.222-0.281	0.14-0.57	0.47-1.48	859-6676	0.44-5.00
FIXED BED							
9 (clay)	0.35-0.75	0.009-0.017	0.049-0.107	0.29-0.60	0.88-1.60	2049-6942	0.13-0.69
9* (clay loam)	0.21-0.74	0.009-0.022	0.079-0.125	0.32-0.64	0.86-1.52	3293-9975	0.17-0.62
15*	0.22-0.72	0.006-0.024	0.128-0.160	0.34-1.31	0.93-3.54	2266-14430	0.05-0.76
22	0.31-0.64	0.006-0.018	0.092-0.219	0.30-0.49	0.85-1.99	1850-5495	0.13-1.28
24	0.25-0.87	0.009-0.024	0.128-0.232	0.36-0.79	1.03-2.01	2554-11641	0.16-0.87
25	0.20-0.87	0.009-0.025	0.196-0.257	0.28-0.79	0.88-2.22	2337-12488	0.19-1.66
26	0.55-0.85	0.010-0.028	0.235-0.298	0.28-0.77	0.61-2.45	3224-9792	0.25-3.29
MOBILE BED, STEP-POOL							
14	0.10-0.30	0.009-0.020	0.097-0.165	0.18-0.38	0.47-0.98	1596-5688	0.45-2.52
22	0.22-0.28	0.009-0.016	0.138-0.219	0.20-0.28	0.54-0.87	1636-3245	0.71-3.28
24	0.41-0.70	0.015-0.031	0.089-0.230	0.32-0.43	0.59-1.01	4005-8241	0.44-2.20
26	0.35-0.86	0.017-0.031	0.191-0.301	0.22-0.42	0.52-0.97	3035-8238	1.17-3.76
FIXED BED, STEP-POOL							
24	0.11-0.71	0.009-0.021	0.150-0.231	0.27-0.87	0.77-1.90	2192-14532	0.23-1.78
26	0.26-0.52	0.007-0.014	0.242-0.303	0.20-0.56	0.69-1.60	1278-5501	0.58-3.06

* Runs carried out fixing rills after the shaping phase.

4. RESULTS

4.1. *Flow resistance law for mobile flat bed rills*

To study the flow resistance in mobile flat bed rills, in which *grain*-resistance and resistance due to sediment transport occur, all the measurements obtained during mobile bed runs (without bed forms) were used. In particular, the available data base was constituted by the runs carried out for slope values equal to 9 (clay), 9 (clay loam), 14, 15, 18, 22, 24, 25 and 26% (437 runs). Furthermore, the literature data (35 runs) by Jiang et al. (2018) were used to widen the available database. This investigation (472 experimental runs) is thus characterized by different texture characteristics and a wide range of the Reynolds ($639 \leq Re \leq 14945$) and Froude number ($0.47 \leq F \leq 8.14$) (Figure 20).

The equation for estimating the Γ_v function was calibrated and tested using two different groups of measurements extracted from the available database. The dataset of calibration was constituted by 355 runs corresponding to the measurements characterized by s_p = 9 (clay), 14, 18, 22, 24, 25 and 26% (320 runs) and those by Jiang et al. (2018) (35 runs). The testing dataset was composed by 117 experimental runs carried out on clay loam (CL) soil with s_p = 9 and 15%.

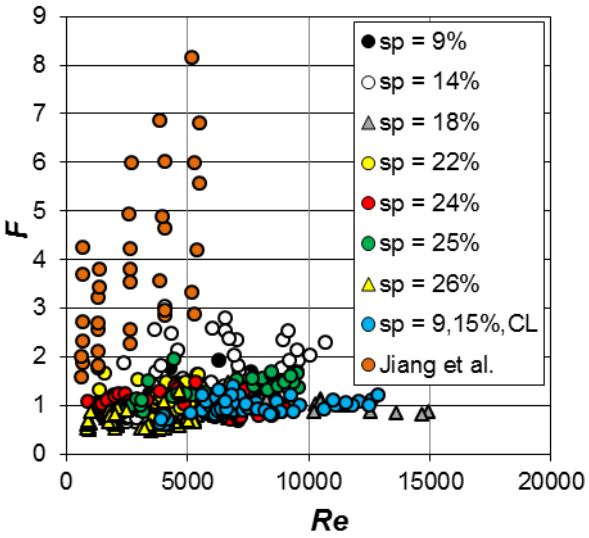

Figure 20. Relationship *Re*-*F* for the experimental runs.

The calibration of Eq. (30) gave the following result:

$$\Gamma_v = \left(\frac{0.4595 CLAY^{0.0381}}{SILT^{0.0275}}\right) \frac{F^{1.0581}}{s^{0.5443}} \qquad (31)$$

in which *CLAY* is the clay content (%) and *SILT* is the silt content (%). Eq. (31) is characterized by a coefficient of determination equal to 0.989 and is applicable for

Reynolds numbers ranging from 639 to 14945, $0.47 \leq F \leq 8.14$, slope values $7.1 \leq s \leq 84\%$, $3 \leq CLAY \leq 73\%$ and *SILT* ranging from 19.9 to 32.8%.

The comparison between the 355 measured Γ_v values (Eq. 29) of the calibrating database, and those calculated by Eq. (31) is plotted in Figure 21.

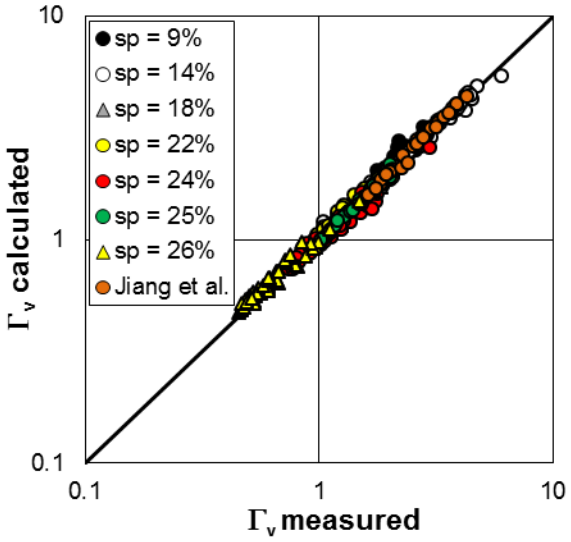

Figure 21. Comparison between the measured Γ_v values (Eq. 29), and those calculated by Eq. (31) for calibration data.

Figure 22 demonstrates that Eq. (31) is positively tested by the flow velocity, depth and slope measurements belonging to the testing dataset (117 experimental runs) for which $0.6 \leq F \leq 1.7$, s varies from 5.1 to 22.8 %, $CLAY = 32.7\%$ and $SILT = 30.9\%$.

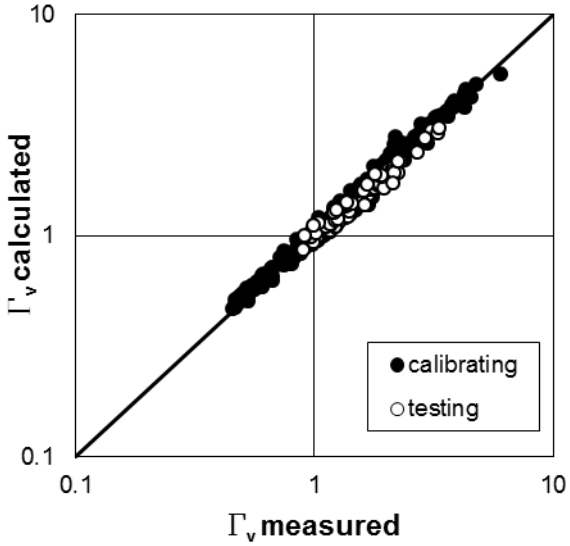

Figure 22. Comparison between the measured Γ_v values and those calculated by Eq. (31) for testing data.

The following flow resistance law was obtained substituting Eq. (31) into Eq. (24):

$$f = 8\left[\frac{(\delta+1)\,(\delta+2)}{2^{1-\delta}\ Re^{\delta}}\left(\frac{SILT^{0.0275}}{0.4595CLAY^{0.0381}}\right)\frac{s^{0.5443}}{F^{1.0581}}\right]^{2/(1+\delta)} \quad (32)$$

According to Eq. (32), the friction factor f increases with the percentage of silt and decreases with clay content of the soil in which the rills are shaped. As the silt particles are easily detachable from the soil mass, the silt fraction is representative of the detachability effect on flow resistance. On the contrary, the primary clay particles are easily transportable, and the clay fraction expresses the effect of transportability on flow resistance. For a fixed sand content, a high silt fraction is coupled with a low clay percentage and the soil is characterized by high particle detachability and low transportability, resulting in high values of friction factor. The good agreement between the measured friction factor values of the calibrating dataset, and those calculated by Eq. (32) is shown in Figure 23.

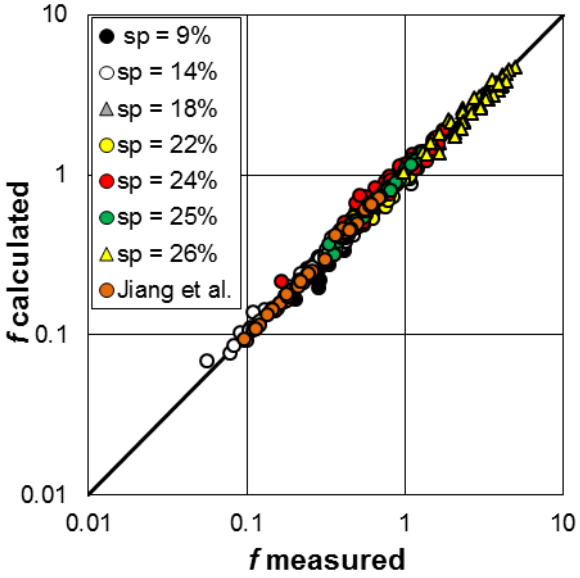

Figure 23. Comparison between measured Darcy-Weisbach friction factor values and those calculated by Eq. (32) for calibration data.

The friction factor values calculated by Eq. (32) are characterized by errors that are less than or equal to ± 20% for 95.8% of cases and less than or equal to ± 10% for 74.1% of cases. Eq. (32) was also positively tested by the flow velocity, depth and slope measurements belonging to the testing dataset (Figure 24).

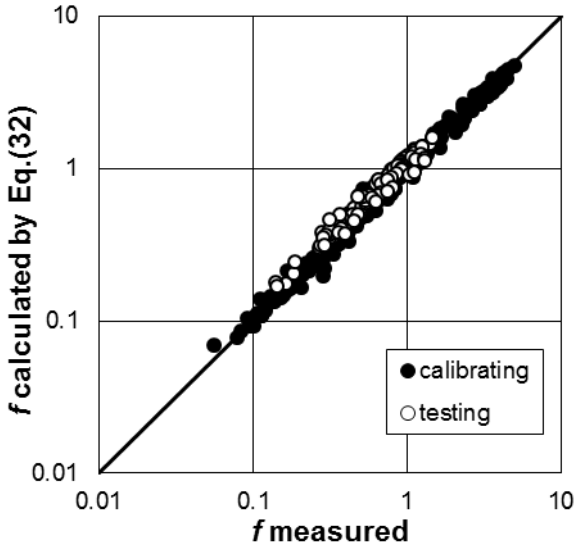

Figure 24. Comparison between measured Darcy-Weisbach friction factor values and those calculated by Eq. (32) for testing data.

Figure 25 shows the relationship between the Reynolds number and the ratio $2c/(\delta+1)$, with c=0.5443, which is the exponent of the slope gradient in Eq. (32). This figure demonstrates that, for the available data base of this investigation (472 experimental runs), the exponent of the slope gradient assumes values ranging from 0.88 to 0.94.

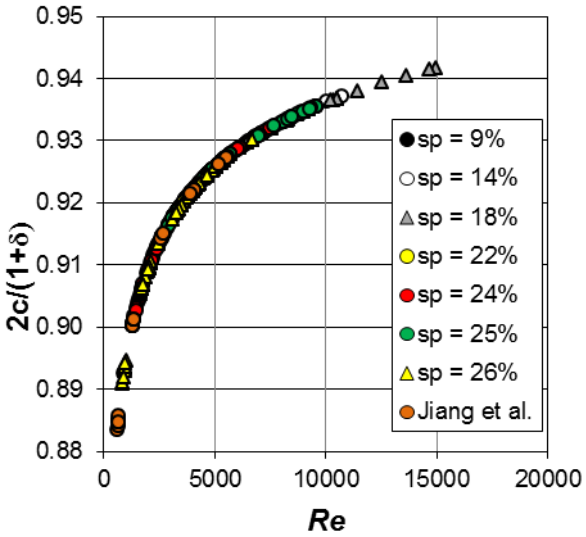

Figure 25. Relationship between the Reynolds number and the exponent of the slope gradient in Eq. (32).

4.2. *Flow resistance law for step-pool rills*

The investigation on flow resistance for step-pool rills was carried out using the measurements obtained for s_p = 14, 22, 24 and 26% for mobile bed runs and s_p = 24 and 26% for fixed bed runs. For mobile bed experiments the total tested reaches are 136 and the measurements, except for a single run ($F = 1.01$), were carried out for the condition of subcritical flow ($0.47 \leq F \leq 0.98$), for transition and turbulent flow regime ($1596 \leq Re \leq 8241$) (Figure 26) and for a small-scale roughness condition ($h/d_{50} \gg 10$, being d_{50} the size at which 50% of the distribution is finer-grained).

For fixed bed experiments the total tested reaches are 63 and the measurements were carried out for the condition of subcritical and supercritical flow ($0.69 \leq F \leq 1.90$) and for transition and turbulent flow regime ($1278 \leq Re \leq 14532$).

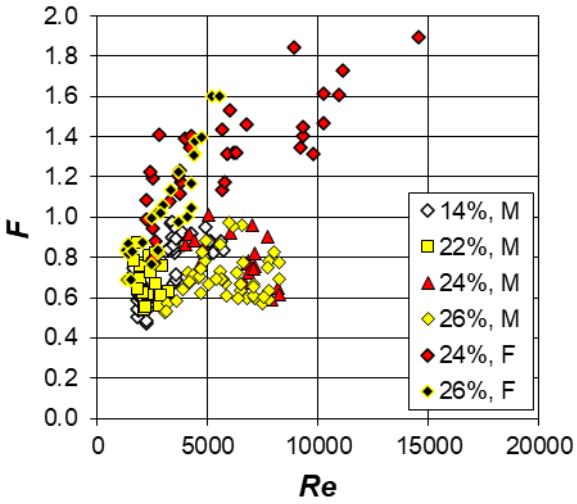

Figure 26. Relationship between the Reynolds number and Froude number for step-pool rills.

Using the measurements corresponding to the 88 mobile rill reaches shaped on the plot having a slope equal to 14, 22 and 24%, the following equation was obtained for step-pool rills:

$$\Gamma_v = 0.4272 \frac{F^{1.0955}}{s^{0.65}} \qquad (33)$$

Eq. (33) for estimating Γ_v was also positively tested by the measurements carried out in 48 mobile rill reaches shaped on the 26% sloped-plot and 63 fixed rill reaches shaped on the 24 and 26% sloping plots (Figure 27).

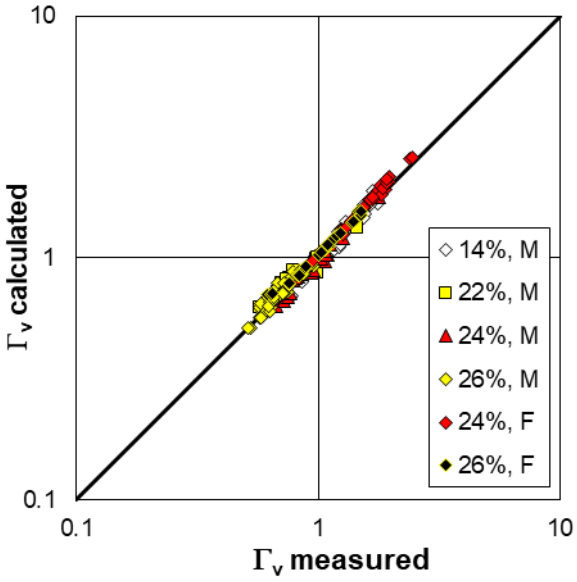

Figure 27. Comparison between the measured Γ_v values (Eq. 29) and those calculated by Eq. (33) for calibration and testing datasets (M=mobile bed; F=fixed bed).

The flow resistance equation (Eq. 24), with δ calculated by Eq. (23) and Γ_v estimated by Eq. (33), tested by the complete data base of 199 investigated rill reaches, can be rewritten in the following way:

$$f = 8\left[\frac{(\delta+1)\,(\delta+2)}{2^{1-\delta}\ Re^{\delta}}\ \frac{s^{0.65}}{0.4272F^{1.0955}}\right]^{2/(1+\delta)} \tag{34}$$

Figure 28, which shows the comparison between the measured friction factor values and those calculated by Eq. (34), points out a good agreement which is characterized by a root mean square error RMSE equal to 0.135. Furthermore, for the whole database the estimate errors are less than or equal to ±15% for 88.4% of cases and less than or equal to ±10% for 72.8% of cases.

For mobile bed runs, on the basis of the experimental range of δ (0.166–0.203), the ratio $2/(1+\delta)$ ranges from 1.66 to 1.72. Assuming the mean value of 1.69 and considering that Re^{δ} is always equal to 4.4817, Eq. (34) can be rewritten as:

$$f = 2.67\left[\frac{(\delta+1)\,(\delta+2)}{2^{1-\delta}}\right]^{1.69}\frac{s^{1.1}}{F^{1.85}} \tag{35}$$

To compare the friction factor values for flat bed and step-pool rills, the results by Di Stefano et al. (2018b) for flat bed mobile rills were used. According to these Authors, the following relationship is applicable for the flat bed condition:

$$f = 2.15\left[\frac{(\delta+1)\,(\delta+2)}{2^{1-\delta}}\right]^{1.69}\frac{s^{0.91}}{F^{1.88}} \tag{36}$$

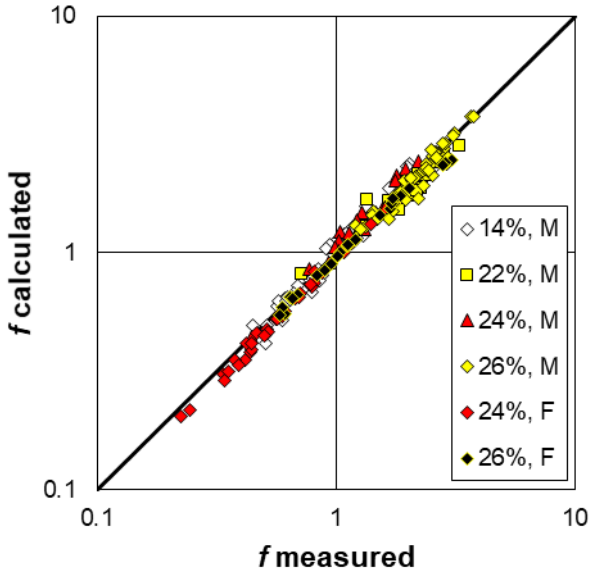

Figure 28. Comparison between the measured *f* values and those calculated by Eq. (34).

4.3. *The effect of sediment transport on flow resistance*

To investigate the contribution of sediment transport on total flow resistance, the comparison between fixed and mobile flat bed rills was performed using two different databases.

The first database included the runs carried out with slope values s_p equal to 9 (clay), 14, 18, 22, 24, 25 and 26% for mobile bed rills and equal to 9 (clay), 22, 24, 25, and 26% for the fixed bed ones. As forementioned, these runs were carried out fixing existing rills after the corresponding mobile bed runs. The available database was constituted by 320 experimental runs for mobile bed and 165 for fixed one. The mobile bed runs are characterized by laminar, transition and turbulent flow regime ($859 \leq Re \leq 14945$) and both subcritical and supercritical flows ($0.47 \leq F \leq 3.03$). Instead, the fixed bed experiments are characterized by Reynolds numbers varying from 1850 to 12488 (transition and turbulent flow regime) and Froude numbers varying from 0.61 to 2.45 (subcritical and supercritical flows). The ranges of Reynolds and Froude number are represented in Figure 29. In this figure, the data by Abrahams et al. (1996), obtained for fixed bed rills, are also reported since these data will be part of the testing database. These data are characterized by Reynolds and Froude number corresponding to transition and turbulent flows ($868 \leq Re \leq 5058$) and to subcritical conditions ($0.31 \leq F \leq 0.91$).

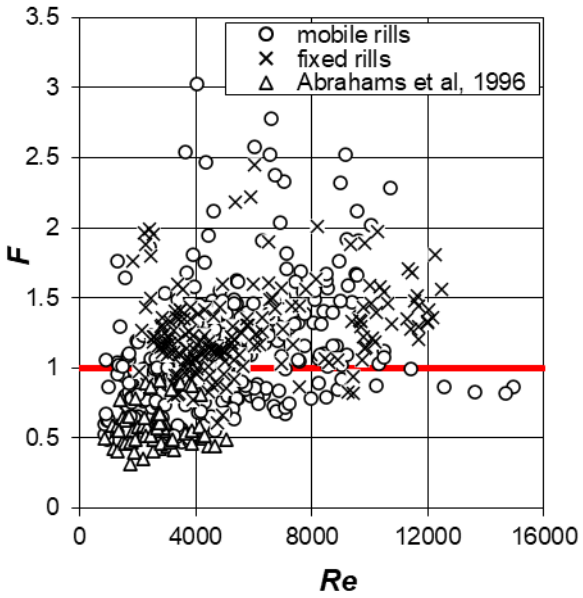

Figure 29. Relationship between the Reynolds number and Froude number for mobile and fixed bed rills.

At first, the following equation for estimating the Γ_v function (Eq. 30) was calibrated using 320 data corresponding to the mobile bed runs:

$$\Gamma_v = 0.5112 \frac{F^{1.0814}}{s^{0.5240}} \quad (37)$$

Eq. (37) is characterized by a coefficient of determination equal to 0.988, and it is applicable for flow Reynolds numbers of $859 \leq Re \leq 14945$, Froude numbers of $0.47 \leq F \leq 3.03$, and slope s values ranging from 7.1% to 28.1%. Figure 30 shows the comparison between the 320 measured Γ_v values (Eq. 29) and those calculated by Eq. (37).

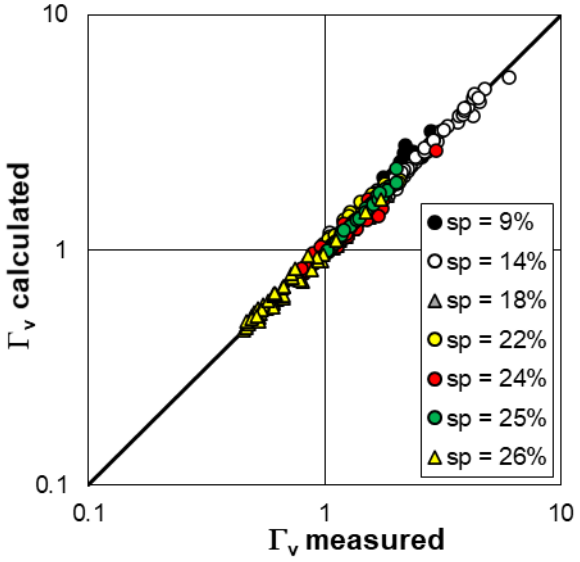

Figure 30. Comparison between the measured Γ_v values (Eq. 29) and those calculated by Eq. (37) for mobile bed rills.

From Eq. (24) and Eq. (37) follows:

$$f = 8\left[\frac{(\delta+1)\,(\delta+2)}{2^{1-\delta}\ 2.291}\ \frac{s^{0.524}}{F^{1.0814}}\right]^{2/(1+\delta)} \tag{38}$$

Figure 31 shows the good agreement between the measured friction factor values and those calculated by Eq. (38) which is characterized by a RMSE equal to 0.108. The estimate errors of Eq. (38) are less than or equal to ±20% for 96.6% of cases and less than or equal to ±10% for 76.6% of cases.

By using Eq. (23) and the experimental values of *Re*, the calculated δ values range from 0.156 to 0.222 and have a mean value of 0.1807. Therefore, setting δ equal to 0.1807, Eq. (38) can be rewritten as follows:

$$f = 3.7652\,\frac{s^{0.888}}{F^{1.8318}} \tag{39}$$

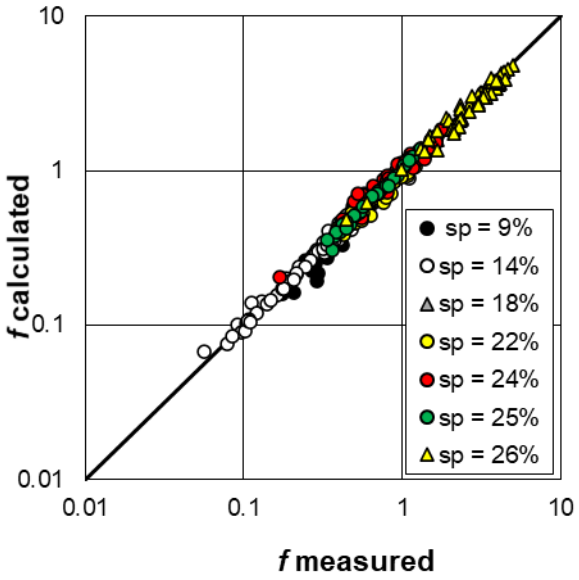

Figure 31. Comparison between the measured friction factor values and those calculated by Eq. (38) for mobile bed rills.

For fixed bed rills, instead, the following equation was obtained:

$$\Gamma_v = 0.4972\,\frac{F^{1.1656}}{s^{0.5310}} \tag{40}$$

Eq. (40) is characterized by a coefficient of determination equal to 0.983, and it is applicable for flow Reynolds numbers of 1850 ≤ *Re* ≤ 12488, Froude numbers of 0.61 ≤ *F* ≤ 2.45, and slope s_p values ranging from 4.9% to 29.8%. Figure 32 shows the comparison between the 165 measured Γ_v values (Eq. 29) and those calculated by Eq. (40).

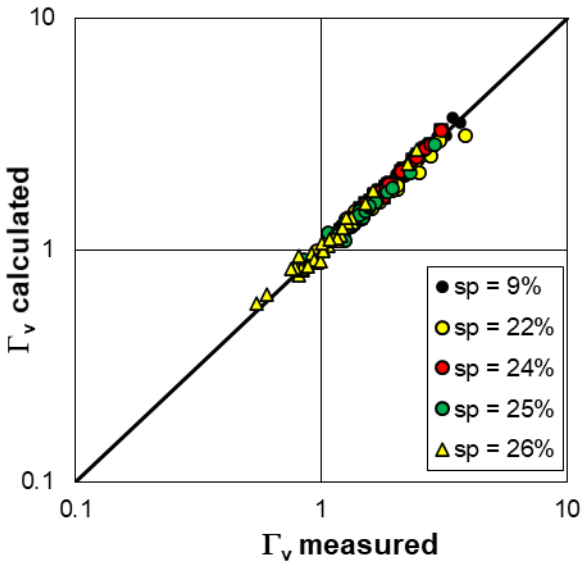

Figure 32. Comparison between the measured Γ_v values (Eq. 29) and those calculated by Eq. (40) for fixed bed rills.

Figure 33 shows the good agreement between the measured friction factor values and those calculated by Eq. (24) coupled with Eqs. (23) and (40). These last values are characterized by errors less than or equal to ±20% for 96.7% of cases and less than or equal to ±10% for 83.6% of cases.

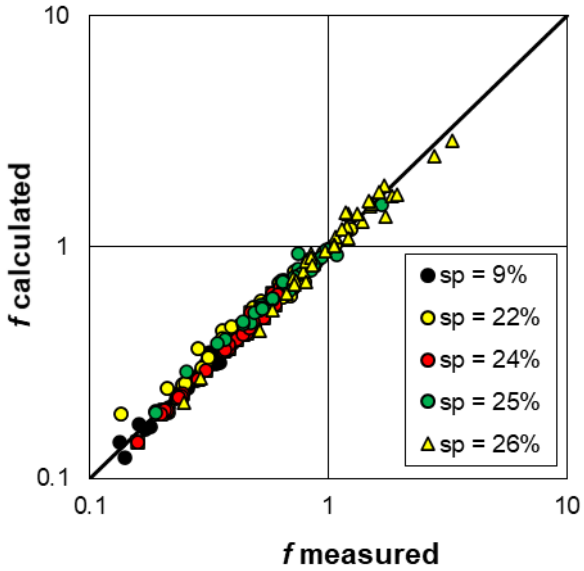

Figure 33. Comparison between the measured friction factor values and those calculated by Eq. (24) coupled with Eqs. (23) and (40) for fixed bed rills.

Taking into account that for the experimental values of *Re*, the calculated δ values (Eq. 23) range from 0.159 to 0.199, and setting δ equal to the mean value of 0.176, Eq. (24) coupled with Eq. (40) can be rewritten as follows:

$$f = 4.1864 \frac{s^{0.903}}{F^{1.1982}} \tag{41}$$

The comparison between Γ_v function for mobile (Eq. 37) and fixed (Eq. 40) bed rills shows that the estimated *a*, *b*, and *c* coefficients are very similar. In fact, Figure 34 shows the good agreement between the 165 measured Γ_v values (Eq. 29) for the fixed bed rills and those calculated by Eq. (37) which was calibrated by the mobile bed rill measurements.

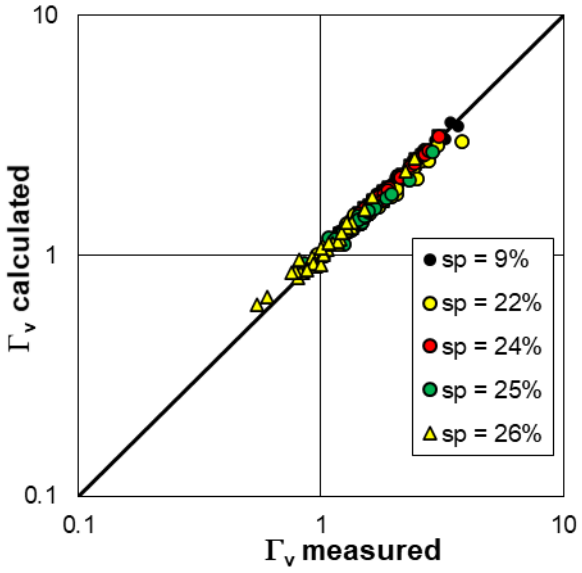

Figure 34. Comparison between the measured Γ_v values (Eq. 29) for fixed bed rills and those calculated by Eq. (37), calibrated by mobile bed rill measurements.

Figure 35 shows the good agreement (RMSE = 0.091) between the measured friction factor values for fixed bed rills and those calculated by Eq. (38), which was calibrated by mobile bed rill data. Eq. (38), applied to the investigated fixed bed rills, is characterized by errors that are less than or equal to ±20% for 95.6% of cases and less than or equal to ±10% for 79.8% of cases.

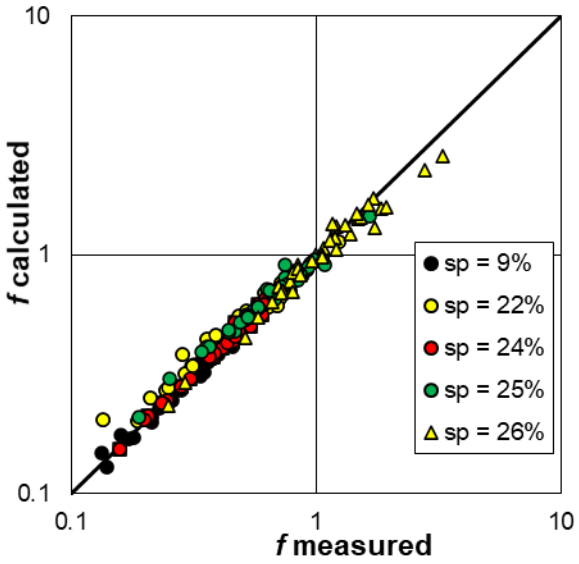

Figure 35. Comparison between the measured friction factor values for fixed bed rills and those calculated by Eq. (38).

For obtaining the component, f_t, of the Darcy–Weisbach friction factor due to the effect of the sediment transport on flow resistance, the difference between the measured f value on the mobile bed rill condition and that of the fixed bed in the same hydraulic condition (Eqs. (24), (23), and (40)) was calculated. Indeed, the former is affected by grain resistance and sediment transport, while the latter is only affected by grain resistance. This f_t value is negligible for 64% of the measured values and the f_t /f ratio is less than or equal to 0.06 for 80.0% of cases (Figure 36).

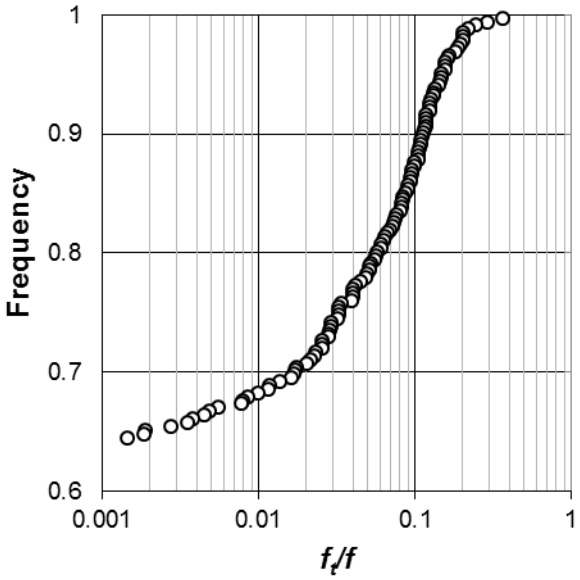

Figure 36. Frequency distribution of the f_t/f ratio.

The second database included the measurements carried out for plot slopes equal to 9 (clay loam) and 15% for both mobile and fixed bed rills. In this last case, the runs were carried out fixing the rills after the shaping phase. The data by Jiang et al. (2018) were also included into this database. For mobile bed condition the experimental runs are thus characterized by a wide range of the Reynolds ($639 \leq Re \leq 12895$) and Froude number ($0.60 \leq F \leq 8.14$). For fixed bed condition the experimental runs are characterized by flow Reynolds numbers of $2266 \leq Re \leq 14330$, Froude numbers of $0.86 \leq F \leq 3.54$.

At first, the measurements carried out in this investigation for the fixed bed rills were used to calibrate Eq. (30) obtaining the following equation:

$$\Gamma_v = 0.4842 \frac{F^{1.1299}}{s^{0.551}} \tag{42}$$

which is characterized by a coefficient of determination equal to 0.983. The comparison between the 72 measured Γ_v values (Eq. 29) and those calculated by Eq. (42) is shown in Figure 37.

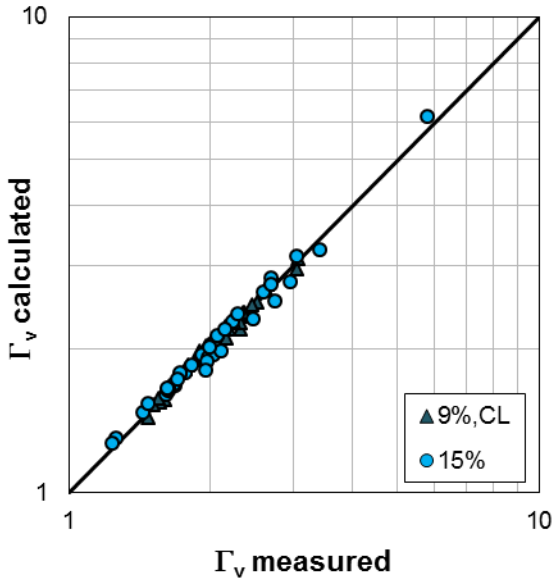

Figure 37. Comparison between the measured Γ_v values (Eq. 29) and those calculated by Eq. (42) for fixed bed rills.

Substituting Eq. (42) into Eq. (24) the following flow resistance equation for a fixed bed rill is obtained:

$$f = 8 \left[\frac{(\delta+1)\,(\delta+2)}{2^{1-\delta}\ Re^{\delta}\ 0.4842} \ \frac{s^{0.551}}{F^{1.1299}} \right]^{2/(1+\delta)} \tag{43}$$

Figure 38 shows the good agreement between the 72 measured f values and those calculated by Eq. (43), which is characterized by a *RMSE* equal to 0.0175 and errors that are always less than or equal to ± 20% and less than or equal to ± 10% for 91.7% of cases.

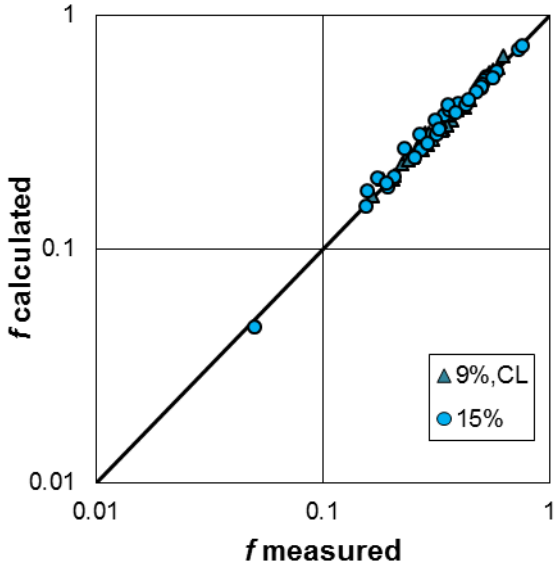

Figure 38. Comparison between the measured f values and those calculated by Eq. (43) for fixed bed rills.

Using a constant value of δ equal to the mean experimental value of 0.171 as its experimental range (0.157-0.194) is narrow, Eq. (43) can be rewritten as follows:

$$f = 3.9292 \ \frac{s^{0.941}}{F^{1.9299}} \qquad (44)$$

The component f_t of the Darcy-Weisbach friction factor was calculated as difference between the f values measured in the mobile bed rills and those calculated in the same hydraulic conditions for fixed bed rills using Eqs. (23) and (43). Figure 39 shows the empirical cumulative frequency distribution of the ratio f_t/f.

Figure 40 shows the comparison between the applied discharge Q with the corresponding ratio f_t /f and the total eroded rill volume RV (m^3). This volume was calculated using the difference of DEMs related to the end of the shaping phase (D_1) and experimental run (D_2), respectively.

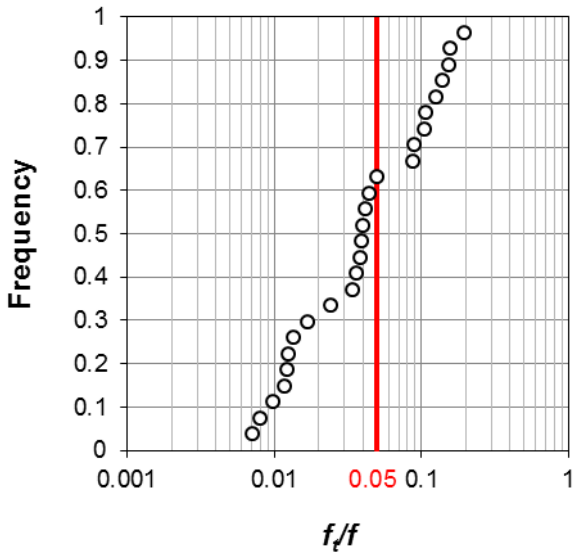

Figure 39. Frequency distribution of the f_t /f ratio.

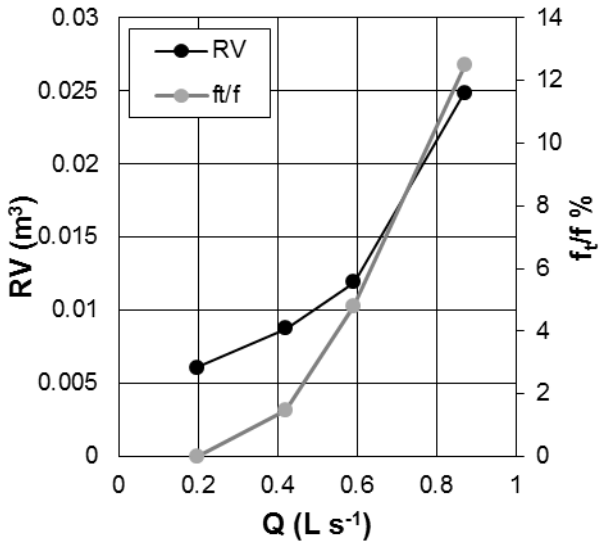

Figure 40. Comparison between the applied discharge Q (L s^{-1}) with the corresponding ratio f_t/f and the total eroded rill volume RV (m^3).

The measurements carried out in this investigation for the mobile bed rills were also used together with those by Jiang et al. (2018) to calibrate Eq. (30) and the following equation was obtained:

$$\Gamma_v = 0.4514 \frac{F^{0.9999}}{S^{0.5935}} \quad (45)$$

which is characterized by a coefficient of determination equal to 0.979. The comparison between the 152 measured Γ_v values (Eq. 29) and those calculated by Eq. (45) is shown in Figure 41.

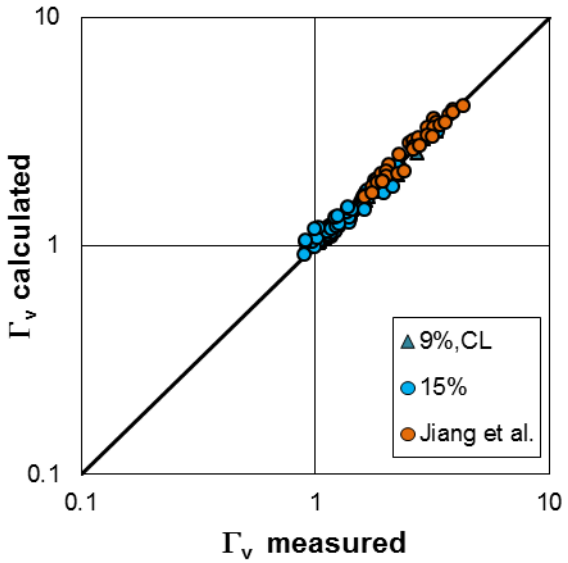

Figure 41. Comparison between the measured Γ_v values (Eq. 29) and those calculated by Eq. (45) for mobile bed rills.

Substituting Eq. (45) into Eq. (24) the following flow resistance equation for a mobile bed rill is obtained:

$$f = 8\left[\frac{(\delta+1)\,(\delta+2)}{2^{1-\delta}\ Re^{\delta}\ 0.4514}\ \frac{s^{0.5935}}{F^{0.9999}}\right]^{2/(1+\delta)} \qquad (46)$$

Figure 42 shows the good agreement between the 152 measured friction factor *f* values and those calculated by Eq. (46), which is characterized by a *RMSE* equal to 0.062 and errors that are less than or equal to $\pm$ 20% for 94.7% of cases and less than or equal to $\pm$ 10% for 78.3% of cases.

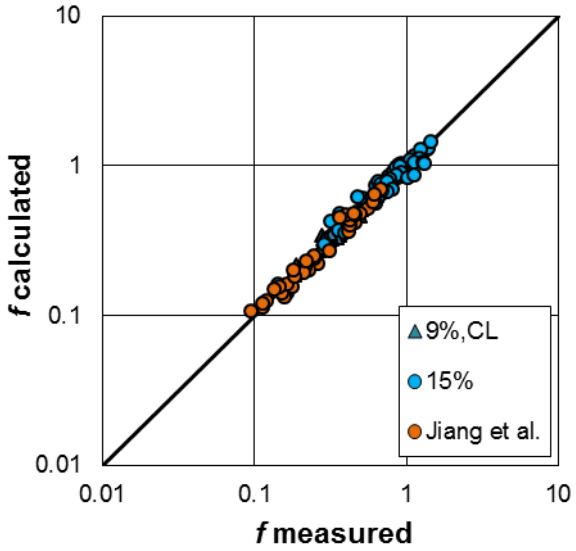

Figure 42. Comparison between the measured *f* values and those calculated by Eq. (46) for mobile bed rills.

Using a constant value of δ equal to the experimental mean value of 0.177 as its experimental range (0.158-0.232) is narrow, Eq. (46) can be rewritten as follows:

$$f = 4.5346 \ \frac{s^{1.008}}{F^{1.6992}} \quad (47)$$

In Table 3 the equations for estimating the Darcy-Weisbach friction factor obtained for all the examined cases are summarized.

Table 3. Equations to estimate the Darcy-Weisbach friction factor for all examined cases.

sub-chapter	*examined case*	*equation*	
1	mobile bed	$f = 8\left[\frac{(\delta+1)\,(\delta+2)}{2^{1-\delta}\ Re^{\delta}}\left(\frac{SILT^{0.0275}}{0.4595CLAY^{0.0381}}\right)\frac{s^{0.5443}}{F^{1.0581}}\right]^{2/(1+\delta)}$	(32)
2	step-pool	$f = 2.67\left[\frac{(\delta+1)\,(\delta+2)}{2^{1-\delta}}\right]^{1.69}\frac{s^{1.1}}{F^{1.85}}$	(35)
3	mobile bed, database 1	$f = 3.7652\frac{s^{0.888}}{F^{1.8318}}$	(39)
3	fixed bed, database 1	$f = 4.1864\frac{s^{0.903}}{F^{1.1982}}$	(41)
3	fixed bed, database 2	$f = 3.9292\ \frac{s^{0.941}}{F^{1.9299}}$	(44)
3	mobile bed, database 2	$f = 4.5346\ \frac{s^{1.008}}{F^{1.6992}}$	(47)

5. DISCUSSION

5.1. *Flow resistance law for mobile flat bed rills*

Eq. (31), which relates Γ_v with slope, Froude number and soil texture, is characterized by a wide range of applicability in terms of flow regime ($639 \leq Re \leq 14945$), flow characteristics ($0.47 \leq F \leq 8.14$) (Figure 20) and slope ($9 \leq s_p \leq 84\%$). The analysis demonstrated that clay and silt fractions of the investigated soils are sufficient for representing the effect of erosion and transport of soil particles on rill flow velocity. According to Eq. (32) (Table 3), the friction factor increases when silt fraction increases (high detachability) and clay fraction decreases (low transportability). In other words, this result expresses that the increase of flow resistance due to *sediment load* is affected by

both soil detachability and transportability. For given hydraulic conditions (water depth h, discharge Q), a high soil detachability (high silt fraction) implies that a relevant part of flow energy is dissipated to detach particles from soil mass. A low soil particle transportability (low clay fraction) implies that an appreciable part of flow energy has to be used to transport coarse (sand fraction) and medium-size (silt fraction) particles. For a fixed sand content, taking into account that a high silt fraction and a low clay percentage are coupled, Eq. (32) states that the increase of Darcy-Weisbach friction factor is due to a contemporaneous occurrence of a high soil particle detachability and a low transportability. The decreasing trend of Darcy-Weisbach friction factor with clay fraction is opposite to that obtained by Palmeri et al. (2018). This discrepancy could be justified taking into account that, for calibrating the relationship between Γ_v and the other variables included in Eq. (31), Palmeri et al. (2018) also used literature data by Strohmeier et al. (2014) and Peng et al. (2015). These last data were obtained by investigations carried out in laboratory flumes appreciably wider than rills, in which most of the experiments (19 out 25) were conducted under a free developed rill condition. Free developed rills are the result of unconstrained rill erosion experienced on a plane soil bed. This experimental condition differs from that of a manually incised straight rill successively shaped by flow, which is characteristic of the other calibrating measurements. Although only 13% of the entire calibrating data base corresponded to a free developed rill condition, these measurements were characterized by a clay fraction range (9.6-19%) significantly different from that related to all the others (42-73%); this difference may have determined the contrasting result with the present one.

According to previous studies (Di Stefano et al., 2017a; 2018; Palmeri et al., 2018), Figure 25 demonstrates that the Darcy-Weisbach friction factor f increases with a power of slope gradient having an exponent close to 1. In other words, this result confirms the hypothesis of Govers (1992) that flow velocity in mobile bed rills is nearly independent of slope. This result is due to a "feedback mechanism" since when slope gradient increases the expected increase of flow velocity is counterbalanced by the increase of bed roughness due to a more active rill erosion process.

5.2. *Flow resistance law for step-pool rills*

Eq. (34) gave good results for mobile bed rills and was positively tested for fixed bed rills. The applicability of this equation, calibrated for mobile bed rills, to measurements obtained for fixed bed condition is explainable since the effect of sediment transport on the flow resistance law can be considered negligible respect to the form-induced flow resistance (*spill resistance*) due to the presence of step-pools structures.

The comparison between the scale factor of Eq. (35) (equal to 2.67) and Eq. (36) (equal to 2.15) confirms that the step-pool configuration is characterized by Darcy-Weisbach friction factor values higher than those obtained for mobile rills with a flat bed.

Eq. (35) shows that the Darcy-Weisbach friction factor increases with the power of slope gradient characterized by an exponent close to 1. This result suggests that a slope independence hypothesis of rill flow velocity, which was already detected for flat bed rills (Figure 25, Eq. 36), also holds for step-pool rills.

In conclusion, if a suitable calibration of the Γ relationship (Eq. 30) is carried out, the theoretical flow resistance equation (Eq. 24) is also applicable for step-pool rills.

5.3. *The effect of sediment transport on flow resistance*

For the first examined database the detected Froude number values (Figure 29) demonstrate that the flow in mobile bed rills tends to be subcritical ($0.5 \leq F \leq 1.5$), whereas the flow in fixed bed rills tends to be supercritical ($1 \leq F \leq 2.5$).

A Froude number nearly equal to 1 can explain why flow velocity is independent of slope and dependent on discharge. In fact, schematizing the rill cross section as a rectangular having a width B and applying the Lagrange's formula to calculate the velocity V of a critical flow, it results:

$$V = g^{1/2}h^{1/2} = \frac{g^{1/2}Q^{1/3}}{B^{1/3}g^{1/6}} = \left(\frac{g^{1/3}}{B^{1/3}}\right)Q^{0.333} \quad (48)$$

A Froude number, which assumes a value (1.11), on average, quasi-equal to 1, which is the case of the mobile bed rills, corresponds to a hydraulic condition in which the flow velocity only depends on discharge (Eq. 48). The analysis developed at rill scale demonstrated that the flow Froude number F_m of the whole rill flow is, on average, equal to 1.12 for the 37 investigated mobile bed rills and equal to 1.26 for the 18 fixed bed rills (Figure 43).

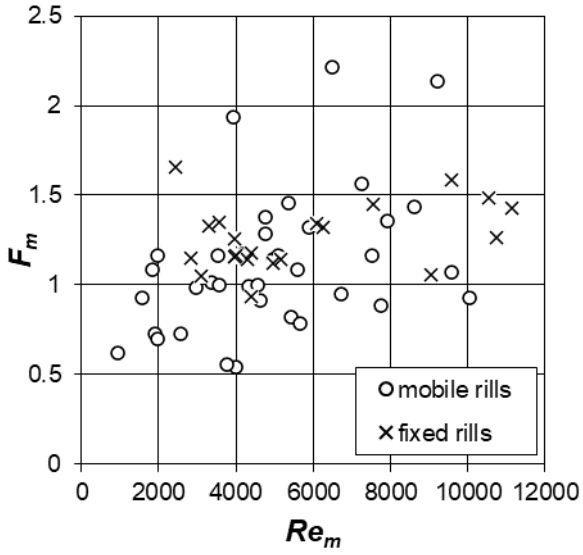

Figure 43. Comparison between the mean values of the Froude number F_m calculated for each mobile bed and fixed bed investigated rill.

Taking into account that for 37 mobile bed rills, the flow is quasi-critical (F_m quasi equal to 1), a slope quasi-independence hypothesis of rill velocity can be correct (Govers, 1992). Mobile bed rills are shaped by flows, which, interacting with the erodible wetted perimeter, are quasi-critical and, as a consequence, the flow velocity is independent of slope. In other words, the feedback mechanism establishes hydraulic conditions, which are that of a quasi-critical flow.

Hessel et al. (2003) suggested an energy-based justification to support the idea that mobile bed rills adjust their geometry (wetted perimeter and roughness) affecting the friction factor values. For increasing values of slope, the rill erosion process becomes more and more relevant and an increasing quote of flow energy is employed for particle detachment from the rill boundary and sediment transport within the rill flow. As a consequence, if erosion-transport phenomena require more energy for increasing slope values, then in a steep slope, less energy will be usable for increasing flow velocity. In mobile bed rills, flow energy, which is dependent on slope, is used both for driving the flow and modifying its kinematic characteristics which in turn are able to modify erosion and transport processes within the rill. In fixed bed rills, flow energy is only employed for driving the rill flow. Therefore, velocities higher than those of mobile bed rills are expected.

Figure 44, which plots the velocity values V versus the energy head $e = h+V^2/2g$, confirms that for a given flow energy the flow velocity in a fixed bed rill tends to be greater than in a mobile bed rill.

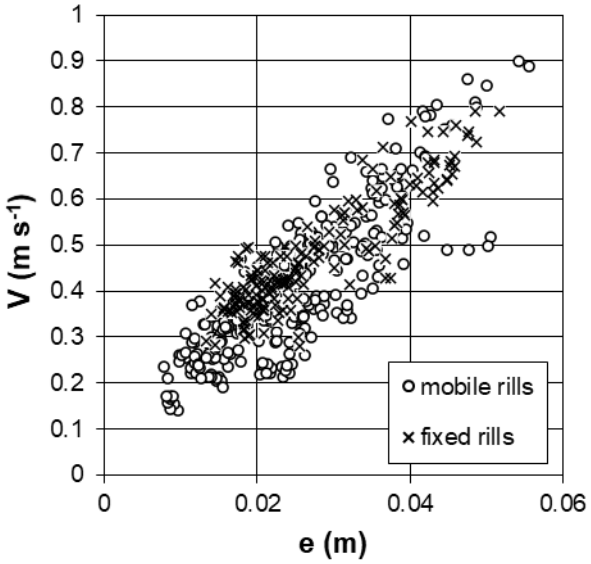

Figure 44. Comparison between velocity values for mobile and fixed bed rills.

If the slope independence of rill velocity hypothesized by Govers (1992) is correct, the Darcy–Weisbach friction factor must linearly increase with s. For mobile bed rills, Eq. (39) shows that the friction factor f increases with the power 0.888 of the slope, whereas Eq. (41) demonstrates that f is proportional to $s^{0.903}$ for fixed bed channels. Therefore, for both channel conditions (mobile and fixed), a negligible influence of slope on rill velocity can be detected. This conclusion can be attributed, in both cases, to the effect of the feedback mechanism. For the mobile bed rills, the expected increase of flow velocity due to slope gradient is counterbalanced by the effect of the increase of erosion rate, which produces an increase of bed roughness, with increasing slope (Govers, 1992). For the fixed bed rills, the experimental runs were carried out fixing a mobile bed channel shaped by flow. The "final" roughness of the mobile bed rill, which increases with rill channel slope, is coincident with the roughness of the fixed bed rill. Therefore, the roughness of the investigated fixed bed rills increases with slope slowing down the flow, and this effect is counterbalanced by the flow velocity increase with slope.

In other words, the feedback effect was frozen fixing the rill bed, and therefore, a slope-independence condition was also imposed for the fixed bed channel. The applicability of the Γ_v function calibrated for the mobile bed rill condition (Eq. 37) to the measurements

carried out for the fixed bed condition further confirms that a fixed bed rill, whose roughness was obtained at the end of a run with mobile bed rill, can be used to detect the feedback effect and the slope-independence condition.

For testing that slope independence of velocity can be recognized by experimental runs carried out in fixed bed rills, the literature data by Abrahams et al. (1996) were also used.

For the fixed bed rills investigated by Abrahams et al. (1996), the following equation for estimating Γ_v was obtained (Figure 45):

$$\Gamma_v = 0.4537 \frac{F^{1.2988}}{s^{0.5460}} \quad (49)$$

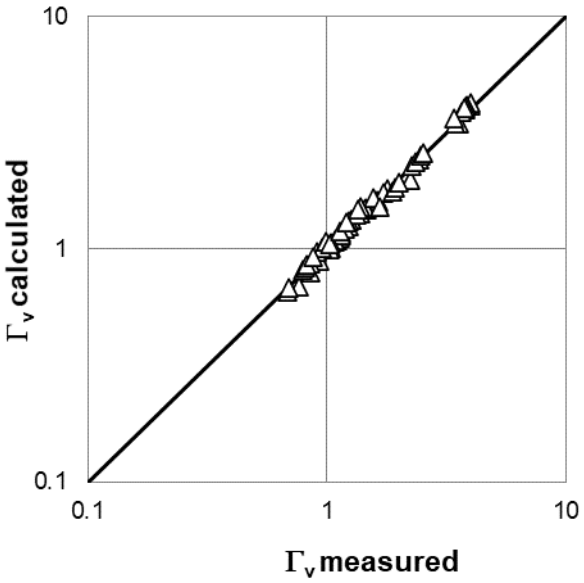

Figure 45. Comparison between the measured Γ_v values (Eq. 29) and those calculated by Eq. (49) for the data by Abrahams et al. (1996).

Figure 46 shows the good agreement between the measured friction factor values and those calculated by Eq. (24) coupled with Eqs. (23) and (49); this comparison is characterized by RMSE equal to 0.08.

Taking into account that for the experimental values of *Re*, the calculated δ values range from 0.176 to 0.222 and setting δ equal to the mean value of 0.193, Eq. (24) coupled with Eq. (49) can be rewritten as follows:

$$f = 4.779 \frac{s^{0.915}}{F^{2.1773}} \quad (50)$$

Therefore, the measurements carried out by Abrahams et al. (1996) confirm a quasi-linear relationship between *f* and *s* and, as a consequence, that a negligible influence of slope on rill velocity can be detected by experimental runs in fixed bed rills.

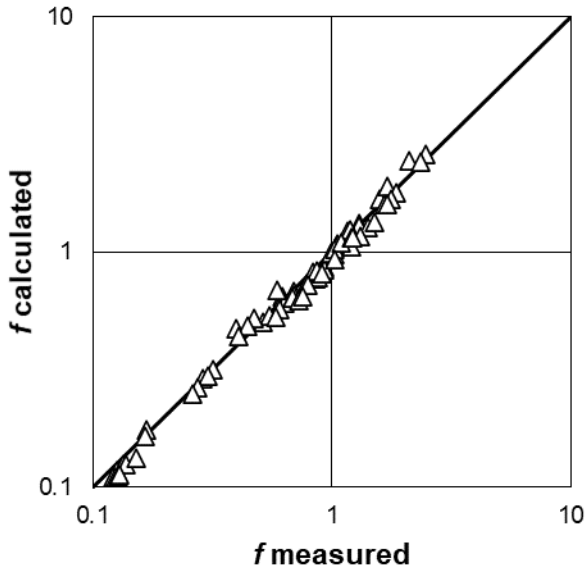

Figure 46. Comparison between measured f values and those calculated by Eq. (24) coupled with Eqs. (23) and (49) for the data by Abrahams et al. (1996).

On the contrary, the experimental runs by Foster et al. (1984), which led to a relationship between rill velocity and slope, did not allow to detect the feedback mechanism because these experiments were carried out by a full sized, fixed bed, fiberglass replica, having a constant roughness, of an actual rill which was placed on a laboratory sloping flume.

Figure 47, showing the data pairs (s, V) for the investigated mobile and fixed rills and for the rills by Abrahams et al. (1996), confirms that the hypothesis of slope independence is also applicable for fixed bed rills when the experimental runs are carried out on rills whose lateral surfaces are fixed after modeling action of a flow.

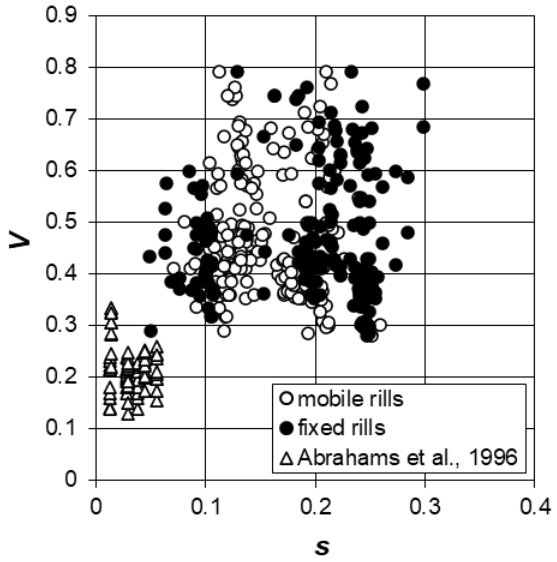

Figure 47. Plot of the data pairs (s, V) for the investigated mobile and fixed rills and for the rills by Abrahams et al. (1996).

The developed analysis concerning the effect of sediment transport on rill resistance showed that only for 20% of the measured friction factor values, the contribution of the sediment transport to the total resistance (grain and sediment transport) is greater than or equal to 6%. In other words, for the investigated conditions, the effect of sediment transport on the flow resistance law can be considered negligible respect to the grain roughness effect.

For the second database and fixed bed rills, Eq. (44) shows that the exponent of s (0.941) is close to 1. According to Eq. (5), the flow velocity in fixed bed rills is independent of channel slope. Since the experimental runs were carried out on rills having fixed bed and walls in which no adjustment of the cross-section geometry was allowed, this result was not expected. For fixed bed rills obtained immobilizing the mobile bed rills at the end of the runs (first database of this investigation) the mean flow velocity was found to be independent of the channel slope. Instead, for this second database no mobile bed runs were carried out before fixing rill beds. Rills were subjected only to a shaping phase due to a clear flow discharge of 0.1 L s^{-1} applied for 3 min before fixing the bed. The circumstance that the mean flow velocity was independent of channel slope in this last experimental condition can be explained by the influence of the initial shaping phase on the fixed bed rill roughness. In particular, during the shaping phase, the increase of flow velocity, due to the increase of plot slope gradient, determined an increase of erosion rate and, consequently, of bed roughness. In other words, a feedback mechanism is "frozen" in this experimental condition as well as in that related to the first database.

Figure 39 demonstrates that the effect of sediment transport on total flow resistance is negligible (f_t/f less than 0.001 for 77.8% of the investigated cases) and the ratio f_t/f is greater than 5% only for 7.7% of the investigated cases. This result agrees with that of the first database.

Figure 40 highlights that when the discharge Q increases the contribution of sediment transport to flow resistance and the eroded rill volume also increase. This result demonstrates that for increasing discharge values the corresponding increase of *sediment load*, due to rill erosion processes, produces an increase of the head losses due to sediment transport with respect to grain resistance. In other words, the effect of sediment transport on flow resistance depends on flow transport capacity which increases with flow discharge. At present, the contribution of sediment transport on rill flow resistance has been little investigated. The study by Di Stefano et al. (2019b) based on measurements by Jiang et al. (2018) established that flow resistance increases with bed load transport, in accordance

with the available results for open channel flows (e.g., Gao and Abrahams, 2004). According to Di Stefano et al. (2019b), the impact of the overall (i.e., bed load and suspended) sediment transport on the flow resistance should be significantly lower than that of the grain roughness.

Eq. (47) demonstrates that in the investigated mobile bed rills the Darcy-Weisbach friction factor increases with slope which surrogates the effect of sediment transport. The exponent of slope (1.008) is close to 1, confirming that a negligible influence of slope on rill velocity occurred.

For a flume having fixed bed and walls with a sediment laden flow, which is the condition investigated by Jiang et al. (2018), when the flume slope increases a gain of both mean flow velocity and transport capacity are expected too. However, in this hydraulic condition, in which the *sediment load* is equal to the transport capacity, the increase of sediment transport requires an increase of flow momentum which is used for the particle transport and this momentum extraction produces flow velocity reduction (Ferro, 2018a). In conclusion, an invariance of mean flow velocity with slope also occurs in this case.

5.4. *Implications and future challenges*

Since, as forementioned, many soil erosion models need the estimate of the flow velocity using Darcy-Weisbach friction factor, the findings of this PhD. dissertation might help to improve the prediction of rill erosion at regional scale. In fact, in this investigation typical Sicilian soils were studied. In particular, the results regarding the clayey soils, which are widely dominant in Sicilian hinterland (characterized by hills and mountains), could be useful to quantify erosive phenomena. In Sicily severe rill erosive events occur mainly during the fall-winter interval, that corresponds to the period in which many areas (especially those cultivated with wheat) are uncovered and consequently more erodible. For this reason, modeling rill erosion can be useful to evaluate if interventions are needed to mitigate the channelized erosion.

In the next future an interesting challenge might be to study the effect of the rill longitudinal profile morphology on flow resistance. Now, in literature there is a lack of research and studies regarding this topic. The past experiments demonstrated that the shape of the rill longitudinal profile is equal to that of the plot. For this reason, the plot might be prepared with a complex longitudinal morphology, characterized by a concave or convex profile.

6. CONCLUSIONS

Experimental studies on rill hydraulics are necessary to determine some characteristics as the mean flow velocity and model rill erosion. Many equations used to describe stream hydraulics are often adapted to rills. The total flow resistance in natural channels is generally constituted by three components: *grain* resistance, due to the shape, the characteristic dimension and the distribution of the elements which determine bed roughness, *morphological* resistance, due to the presence of bed forms as step-pools and resistance due to *sediment load* that determine the loss of flow momentum.

The aim of the present investigation was to calibrate a theoretical resistance equation, (Eq. 24) expressed in terms of Darcy-Weisbach friction factor, using rill measurements. The contribution of the three components of flow resistance was also investigated.

The dimensional analysis and the incomplete self-similarity hypothesis were used to obtain the potential velocity profile, which was integrated to deduce the flow resistance equation in which the Γ function and the exponent of the velocity profile δ are included. The Γ function was determined by experimental measurements carried out in this investigation.

Hydraulic and geometric measurements were carried out for rill reaches shaped by the flow on two plots characterized by different textures and slope gradients. Mobile and fixed bed rills, with both flat bed and step-pools, were used to carry out the experiments.

Using the database constituted by the measurements carried out by Jiang et al. (2018) and by in this investigation for slope values equal to 9 (clay), 14, 18, 22, 24, 25 and 26%, Eq.(30), useful to estimate Γ, was calibrated. This Equation was positively tested by the data obtained for slope values equal to 9 (clay loam) and 15 %. Eq. (32) gave an accurate estimate of the Darcy-Weisbach friction factor, since the calculated values were characterized by errors lower than or equal to ± 20% for 95.8% of cases and lower than or equal to ± 10% for 74.1% of cases. According to the obtained results, flow resistance is affected by both silt and clay fractions that are representative of soil detachability and transportability.

Morphological-resistance was studied using the measurements obtained for s_p = 14, 22, 24 and 26% where step-pool occurred. The theoretical approach (Eq. 34) also ensured a good estimate of the Darcy-Weisbach friction factor in this bed morphological condition for both mobile and fixed bed rills. Indeed, the estimate errors were less than or equal to ±15% for 88.4% of cases and less than or equal to ±10% for 72.8% of cases. The applicability of Eq. (34) calibrated for mobile bed rills, to measurements obtained for fixed bed rills is

explainable since the effect of sediment transport on the flow resistance law can be considered negligible respect to the effect due to the presence of step-pool structures. The scale factors of Eqs. (35) and (36) confirmed that the step-pool configuration is characterized by Darcy-Weisbach friction factor values higher than those obtained for mobile flat bed rills.

Two comparisons between the runs carried out on mobile and fixed bed rills for two different databases allowed to evaluate the component of the resistance due to sediment transport to total flow resistance. For the tested experimental conditions, the theoretical approach resulted successful, and this component resulted often negligible.

In all examined cases the "feedback mechanism" suggested by Govers (1992), for which the mean flow velocity is independent of slope gradient, was confirmed. For fixed bed rills this result can be justified by a "frozen" feedback mechanism caused by mobile bed runs carried out before fixing rills or by the shaping phase.

In conclusion, the theoretical flow resistance law (Eq. 24) was successfully calibrated and tested in different experimental conditions (rills with mobile, fixed, flat and 'step-pool shaped' bed) and was also useful to investigate the sediment transport effect on rill flow resistance.

References

Aberle, J., Smart, G.M., 2003. The influence of roughness structure on flow resistance on steep slopes. *Journal of Hydraulic Research*, 41, 259-269.

Abrahams, A.D., Li, G., Atkinson, J.F., 1995. Step pool streams: adjustment to maximum flow resistance. *Water Resour. Res.*, 31, 2593–2602.

Abrahams, A.D., Gang, L.I, Parsons, A.J., 1996. Rill hydraulics on a semiarid hillslope, southern Arizona. *Earth Surface Processes and Landforms*, 21, 35-47.

Angers, D.A., Caron, J., 1998. Plant-induced changes in soil structure: processes and feedbacks. *Biogeochemistry*, 42 (1–2), 55–72.

Bagarello, V. Ferro, V., 2004. Plot-scale measurements of soil erosion at the experimental area of Sparacia (Southern Italy). *Hydrological Processes*, 18, 141-157.

Bagarello, V., Di Stefano, C., Ferro, V., Pampalone, V., 2015. Establishing a soil loss threshold for limiting rilling. *Journal of Hydrological Engineering*, ASCE, 20, C6014001-1 – C6014001-5.

Bagarello, V., Ferro, V., 2010. Analysis of soil loss data from plots of different length for the Sparacia experimental area, Sicily, Italy. *Byosystems Engineering*, 105, 411-422.

Baiamonte, G., Ferro, V., Giordano, G., 1995. Advances on velocity profile and flow resistance law in gravel bed rivers. *Excerpta*, 9, 41–89.

Baiamonte, G., Ferro, V., 1997.The influence of roughness geometry and Shields parameter on flow resistance in gravel-bed channels. *Earth Surface Processes and Landforms*, 22**,** 759-772.

Barenblatt, G.I., 1979. Similarity, Self-Similarity, and Intermediate Asymptotics, Consultants Bureau Plenum Press New York and London 218.

Barenblatt, G.I., 1987. Dimensional analysis. Gordon & Breach, Science Publishers Inc., Amsterdam.

Barenblatt, G.I., 1991. On the scaling laws (incomplete self-similarity with respect to Reynolds numbers) for the developed turbulent flows in tubes. *C.R. Acad. Sci*., Ser.II 13, 307-312.

Barenblatt, G.I., 1993. Scaling laws for fully developed turbulent shear flows, part 1, Basic hypothesis and analysis. *Journal of Fluid Mechanics*, 248, 513-520.

Barenblatt, G.I., Monin, A.S., 1979. Similarity laws for turbulent stratified flows. *Arch. Ration. Mech. Anal.*, 70, 307-317.

Barenblatt, G.I., Prostokishin, V.M., 1993. Scaling laws for fully developed turbulent shear flows, part 2. Processing of experimental data. *J. Fluid Mech*., 248, 521-529.

Bennet, J., 1999. Effect of slope on the growth and migration of headcuts in rills. *Geomorphology*, Volume 30, Issue 3, Pages 273-290.

Bruno, C., Di Stefano, C., Ferro, V., 2008. Field investigation on rilling in the experimental Sparacia area, South Italy. *Earth Surface Processes and Landforms*, 33, 263-279.

Brunton, D.A., Bryan, R.B., 2000. Rill network development and sediment budgets. *Earth Surface Processes and Landforms*. Volume 25, Issue 7, Pages 783-800.

Campbell, L., McEwan, I., Nikora, V., Pokrajac, D., Gallagher, M., Manes, C., 2005. Bed-load effects on hydrodynamics of rough-bed open-channel flows. *Journal of Hydraulic Engineering*, ASCE, 131, 576-585.

Canovaro, F., Paris, E., Solari, L., 2004. Influence of macro-roughness arrangement on flow regime. In: Greco, M., Caravetta, A., Della Morte, R. (Eds.), *River Flow* 2004. Taylor & Francis, Philadelphia, Pa, pp. 287–293.

Carollo, F.G. , Di Stefano, C., Ferro, V., Pampalone, V., 2015. Measuring rill erosion at plot scale by a drone-based technology. *Hydrol. Process.*, 29, pp. 3802-3811.

Casalí, J., Loizu, J., Campo, M.A., De Santisteban, L.M., Àlvarez – Mozos, J., 2006. Accuracy of methods for field assesment of rill and ephemeral gully erosion. *Catena*, 67, pp. 128-138.

Castaing, B., Gagne, Y., Hopfinger, E.J., 1990. Velocity probability density functions of high Reynolds number turbulence. *Physica D*, 46, 177-200.

Castillo, C., Pérez, R., James, M. R., Quinton, J. N., Taguas, E. V., Gómez, J. A., 2012. Comparing the Accuracy of Several Field Methods for Measuring Gully Erosion. *Soil Science Society of America Journal*, 76(4), 1319. https://doi.org/ 10.2136/sssaj2011.0390.

Chin, A., Wohl, E., 2005. Toward a theory for step pools in stream channels. *Prog. Phys. Geogr*., 29, 275–296.

Chow, VT., 1959. Open-channel hydraulics. McGraw-Hill Book Coo, New York.

Church, M., Zimmermann, A., 2007. Form and stability of step-pool channels: research progress. *Water Resour. Res.*, 43 (W03415), 1–21.

Comiti, F., Andreoli, A., Lenzi, M. A., 2005. Morphological effects of local scouring in step-pool streams. *Earth Surf. Processes Landforms*, 30(12), 1567– 1581.

Comiti, F., Mao, L., Wilcox, A., Wohl, E., Lenzi, M.A., 2007. Field-derived relationships for flow velocity and resistance in high-gradient streams. *J. Hydrol.*, 340, 48–62.

Comiti, F., Cadol, D., Wohl, E., 2009. Flow regimes, bed morphology, and flow resistance in self-formed step-pool channels. *Water Resour. Res.*, 45 (W04421), 1–18.

Curran, J. C., Wilcock, P.R., 2005. Characteristic dimensions of the step-pool bed configurations: An experimental study. *Water Resources Research*, 41, W02030. Doi:10.1029/2004WR00 3568.

D'Agostino, V., Michelini, T., 2015. On kinematics and flow velocity prediction in steppool channels. *Water Resour. Res.*, 51, 4650–4667.

De Roo, A.P.J.D.E., Wesseling, C.G., and Ritsema, C.J., 1996a. LISEM: A single-event physically based hydrological and soil erosion model for drainage basins. I: Theory, input and output. *Hydrological Processes*, 10, 1107–1117.

De Roo, A.P.J., Offermans, R.J.E., and Cremers, N.H.D.T., 1996b. LISEM: A single-event, physically based hydrological and soil erosion model for drainage basins. II: Sensitivity analysis, validation and application, *Hydrological Processes*, 10, 1119–1126, doi:10.1002/(sici)1099-1085(199608)10:8<1119::aid- hyp416>3.0.co;2-v,.

Di Stefano, C., Ferro, V., 2016. Establishing soil loss tolerance: An overview. *Journal of Agricultural Engineering*, 47 (3), art. no. 560, pp. 127-133.

Di Stefano, C., Ferro, V., Pampalone, V., Sanzone, F., 2013. Field investigation of rill and ephemeral gully erosion in the Sparacia experimental area, South Italy. *Catena*, 101, 226–234.

Di Stefano, C., Ferro, V., Pampalone, V., 2015. Modeling rill erosion at the Sparacia experimental area. *J. Hydrol. Eng. ASCE*, 20 (C5014001), 1–12.

Di Stefano, C., Ferro, V., Palmeri, V., Pampalone, V., 2017a. Flow resistance equation for rills. *Hydrological Processes*, 31, 2793-2801, DOI: 10.1002/hyp.11221.

Di Stefano, C., Ferro, V., Palmeri, V., Pampalone, V., Agnello, F., 2017b. Testing the use of an image-based technique to measure gully erosion at Sparacia experimental area. *Hydrol. Process.*, 31 (2017), pp. 573-585.

Di Stefano, C., Ferro, V., Palmeri, V., Pampalone, V., 2017c. Measuring rill erosion using structure from motion: A plot experiment. *Catena*, 156, 383-392, DOI:10.1016/j.catena.2017.04.023.

Di Stefano, C., Ferro, V., Palmeri, V., Pampalone, V., 2018a. Assessing dye-tracer technique for rill flow velocity measurements. *Catena*, 171, 523-532, DOI:10.1016/j.catena.2018.07.044.

Di Stefano, C., Ferro, V., Palmeri, V., Pampalone, V., 2018b. Testing slope effect on flow resistance equation for mobile bed rills. *Hydrological Processes*, 32, 664-671, DOI: 10.1002/hyp.11448.

Di Stefano, C., Palmeri, V., Pampalone, V., 2019a. An automatic approach for rill network extraction to measure rill erosion by terrestrial and low-cost unmanned aerial vehicle photogrammetry. *Hydrological Processes*, 33:1883–1895.

Di Stefano, C., Nicosia, A., Pampalone, V., Palmeri, V., Ferro V., 2019b. Rill flow resistance law under equilibrium bed-load transport conditions. *Hydrological Processes*, 33, 1317–1323. DOI: 10.1002/hyp.13402.

Di Stefano, C., Nicosia, A., Palmeri, V., Pampalone, V., Ferro V., 2020. Dye-tracer technique for rill flows by velocity profile measurements. *Catena*, 185, 104313. https://doi.org/ 10.1016/j.catena.2019.104313.

Emmett, W.W., 1970. The hydraulics of overland flow on hillslopes. *U.S. Geological Survey Professional Papers* 622-A.

Ferro, V., 1997. Applying hypothesis of self-similarity for flow-resistance law of small-diameter plastic pipes. *Journal of Irrigation and Drainage Engineering*, ASCE 123, 175-179.

Ferro, V., 1999. Friction factor for gravel-bed channel with high boulder concentration. *Journal of Hydraulic Engineering*, 125, 771–778. https://doi.org/10.1061/(ASCE) 0733-9429(1999) 125:7(771).

Ferro, V. 2003. ADV measurements of velocity distribution in a gravel bed flume. *Earth Surface Processes and Landforms*, 28, 707-722.

Ferro, V., 2017. New flow resistance law for steep mountain streams based on velocity profile. *Journal of Irrigation and Drainage Engineering*, ASCE 143, 04017024, 1-6, DOI: 10.1061/(ASCE)IR.1943-4774.0001208.

Ferro, V., 2018a. Flow resistance law under equilibrium bed-load transport conditions. *Flow Measurement and Instrumentation*, 64, 1-8, https://doi.org/10.1016/ j.flowmeasinst.2018. 10.008.

Ferro, V., 2018b. Assessing flow resistance in gravel bed channels by dimensional analysis and self-similarity. *Catena*, 169, 119-127. DOI: 10.1016/j.catena.2018.05.034.

Ferro, V., Baiamonte, G., 1994. Flow velocity profiles in gravel bed rivers. *Journal of Hydraulic Engineering*, ASCE, 120, 60-80.

Ferro, V., Giordano, G., 1993. Velocity profile and flow resistance in gravel bed rivers, *Excerpta*, 7, 99-144.

Ferro, V., Nicosia, A., 2020. Comment on “Rill erosion processes on steep colluvial deposit slope under heavy rainfall in flume experiments with artificial rain by F. Jiang et al.”. *Catena*, Volume 185, 103793. https://doi.org/10.1016/j.catena. 2018.10.022.

Ferro, V., Pecoraro, R., 2000. Incomplete self-similarity and flow velocity in gravel bed channels. *Water Resources Research*, 36, 2761-2770.

Ferro, V., Porto, P., 2018. Applying hypothesis of self-similarity for flow resistance law in Calabrian gravel-bed rivers. *Journal of Hydraulic Engineering*, ASCE, 140, 04017061, 1-11, DOI: 10.1061/(ASCE)HY.1943-7900.0001385.

Foster, G.R., Flanagan, D.C., Nearing, M.A., Lane, L.J., Risse, L.M., Finkner, S.C., 1995. Hillslope erosion component. In USDA Water Erosion Prediction Project Hillslope Profile and Watershed Model Documentation (Flanagan D.C., Nearing M.A., Eds.). NSERL Report No. 10. USDA-ARS National Soil Erosion Research Laboratory,West Lafayette, Ind. 12 pp.

Foster, G.R., Huggins, L.F., Meyer, L.D., 1984. A laboratory study of rill hydraulics: I. Velocity relationships. *Transactions of the ASAE*, 27, 790-796.

Foster, G.R., Knisel, W.G., 1981. CREAMS: A Field Scale Model for Evaluating Best Management Practices. Economics, Ethics, Ecology: Roots of Productive Conservation.

Frankl, A., Stal, C., Abraha, A., Nyssen, J., Rieke-Zapp, D., De Wulf, A., Poesen, J., 2015. Detailed recording of gully morphology in 3D through image-based modelling. *Catena*, 127, 92–101.

Gale, W.J., Cambardella, C.A., Bailey, T.B., 2000. Root-derived carbon and the formation and stabilization of aggregates. *Soil Sci. Soc. Am. J.*, 64, 201–207.

Gao, P., Abrahams, A.D., 2004. Bedload transport resistance in rough open-channel flows. *Earth Surface Processes and Landforms*, 29, 423-435.

Gazzolo, T., Bassi, G., 1961. “Contributo allo studio del grado di erodibilità dei terreni costituenti i bacini montani dei corsi d'acqua italiani” in Italian. Giornale del Genio Civile, Roma 4(1).

Gilley, J.E., Kottwitz, E.R., Simanton, J.R., 1990. Hydraulics characteristics of rills. *Transactions of the ASAE*, 27, 797-804.

Giménez, R., Govers, G., 2001. Interaction between bed roughness and flow hydraulics in eroding rills. *Water Resources Research*, 37: 791-799.

Giménez, R., Léonard, J., Duval, Y., Richard, G., Govers, G., 2007. Effect of bed topography on soil aggregates transport by rill flow. *Earth Surface Processes and Landforms*, 32, 4, 602-611. https://doi.org/10.1002/esp.1418.

Glendell, M., McShane, G., Farrow, L., James, M. R., Quinton, J., Anderson, K., Brazier, R. E., 2017. Testing the utility of structure-from-motion photogrammetry reconstructions using small unmanned aerial vehicles and ground photography to estimate the extent of upland soil erosion. *Earth Surface Processes and Landforms*, 42(12), 1860–1871. https://doi.org/ 10.1002/esp.4142.

Gómez-Gutiérrez, A., Schnabel, S., Berenguer-Sempere, F., Lavado-Contador, F., Rubio-Delgado, J., 2014. Using 3D photo-reconstruction methods to estimate gully headcut erosion. *Catena*, 120, 91-101.

Gomiero, T., 2016. Soil Degradation, Land Scarcity and Food Security: Reviewing a Complex Challenge. *Sustainability*, 8, 281; doi:10.3390/su8030281.

Govers, G., 1992. Relationship between discharge, velocity and flow area for rills eroding loose, non –layered materials. *Earth Surface Processes and Landforms*, 17, 515-528.

Govers, G., Takken, I., Helming, K., 2000. Soil roughness and overland flow, *Agronomie*, Volume 20, Number 2, pp 131- 146. https://doi.org/10.1051/agro:2000114.

Govers, G., Gimenez, R., Oost, K.V., 2007. Rill erosion: exploring the relationship between experiments, modeling and field observations. *Earth Science Reviews*, 83, 87-102.

Gyssels, G., Poesen, J., Bochet, E., Li, Y., 2005. Impact of plant roots on the resistance of soils to erosion by water: a review. *SAGE J.*, 29 (2), 189–217.

Hairsine, P.B., Rose, C.W., 1992a. Modeling water erosion due to overland flow using physical principles 1: sheet flow. *Water Resource Research*, 28, 237–243.

Hairsine, P.B., Rose, C.W., 1992b. Modeling water erosion due to overland flow using physical principles 2: rill flow. *Water Resource Research*, 28, 245–250.

Hauge, C.J., 1977. Soil erosion definitions, *California geology*, 30, 202-203.

Hessel, R., Jetten, V., Guanghui, Z., 2003. Estimating Manning's n for steep slopes. *Catena*, 54, 77-91.

James, M.R., Robson, S., 2012. Straightforward reconstruction of 3D surfaces and topography with a camera: accuracy and geoscience application. *J. Geophys. Res.*, 117, F03017. http://dx.doi.org/10.1029/2011jf002289.

Javernick, L., Brasington, J., Caruso, B., 2014. Modeling the topography of shallow braided rivers using structure-from-motion photogrammetry. *Geomorphology*, 213,166–182.

Jiang, F., Gao, P., Si, X., Zhan, Z., Zhang, H., Lin, J., Ji, X., Wang, M.K., Huang, Y., 2018. Modelling the sediment transport capacity of flows in non-erodible rills, *Hydrological Processes*, 32, 26, 3852-3865. https://doi.org/10.1002/hyp.13294.

Knisel, W.G., 1980. CREAMS: A Field-scale Model for Chemicals, Runoff and Erosion from Agricultural Management Systems, *USDA Conservation Research report No. 26*, USDA-ARS, Washington DC, USA.

Leopold, L.B., Maddock, T., 1953. The hydraulic geometry of stream channels and some physiographic implications. Washington: U. S. Geological Survey Professional Paper 252.

Leopold, L.B., Wolman, M.G., Miller, J.P., 1964. Fluvial Processes in Geomorphology. W. H. Freeman and Company, San Francisco, California.

Li, G., Abrahams, A.D., 1997. Effect of salting sediment load on the determination of the mean velocity of overland flow. *Water Resources Research*, 33, 341‐347.

Line, D.E., Meyer, L.D., 1988. Flow velocities of concentrated runoff along cropland furrows. *Transactions of the ASAE*, 31, 1435-1439.

Luk, S. H., Merz, W., 1992. Use of the salt tracing technique to determine the velocity of overland flow. *Soil Technology*, 5, 289–301.

Milzow, C., Molnar, P., McArdell, B.W., Burlando, P., 2006. Spatial organization in the step-pool structure of a steep mountain stream (Vogelbach, Switzerland). *Water Resources Research*, 42, 4. https://doi.org/10.1029/2004WR003870.

Morgan, R.P., Quiton, J.N., Smith, R.E., Govers, G., Poesen, J.W., Auerswald, K., Chisci, G., Torri, D., Stycaen, M.E., 1998. The European soil erosion model (EUROSEM): a dynamic approach for predicting sediment transport from fields and small catchments. *Earth Surface Processes and Landforms*, 23 (6), 527–544.

Mutchler, C.K., Young, R.A., 1975. Soil detachment by raindrops. Present and Prospective Technology for Predicting Sediment Yields and Sources. *ARS*-S-40, pp. 113-117.

Nearing, M.A., Norton, L.D., Bulgakov, D.A., Larionov, G.A., West, L.T., Dontsova, K.M., 1997. Hydraulics and erosion in eroding rills. *Water Resources Research*, 33, 865-876.

Nearing, M.A., Foster, G.R., Lane, L.J., Finkner, S.C., 1989. A process-based soil erosion model for USDA-Water Erosion Prediction Project technology. *Transactions of American Society of Agricultural Engineers*, Vol. 32, 1587-1593.

Nearing, M.A., Simanton, J.R., Norton, L.D., Bulygin, S.I., Stone, J., 1999. Soil erosion by surface water flow on a stony, semiarid hillslope. *Earth Surface Processes and Landforms*, 24 (8), 677 -686.

Nearing, M.A., Polyakov, V.O., Nichols, M.H., Hernandez, M., Li, L., Zhao, Y., Armendariz, G., 2017. Slope–velocity equilibrium and evolution of surface roughness on a stony hillslope. *Hydrol. Earth Syst. Sci.*, 21, 3221–3229.

Nicosia, A., Di Stefano, C., Palmeri, V., Pampalone, V., Ferro, V., 2020a. Flow resistance of overland flow on a smooth bed under simulated rainfall. *Catena*, 187, 104351. https://doi.org/10.1016/j.catena.2019.104351.

Nicosia, A., Di Stefano, C., Pampalone, V., Palmeri, V., Ferro, V., Nearing, M.A., 2020b. Testing a theoretical resistance law for overland flow on a stony hillslope. *Hydrological Processes*, 1-9, DOI: 10.1002/hyp.13709

Nicosia, A., Di Stefano, C., Pampalone, V., Palmeri, V., Ferro, V., Polyakov, V., Nearing, M.A., 2020c. Testing a theoretical resistance law for overland flow under simulated rainfall with different types of vegetation. *Catena*, 189, 104482. https://doi.org/10.1016/j.catena.2020. 104482.

Nouwakpo, S.K., Williams, C.J., Al-Hamdam, O.Z., Weltz, M.A., Pierson, F., Nearing, M., 2016. A review of concentrated flow erosion processes on rangelands: fundamental understanding and knowledge gaps. *International Soil and Water Conservation Research*, 4, 75-86.

Palmeri, V., Pampalone, V., Di Stefano, C., Nicosia, A., Ferro, V., 2018. Experiments for testing soil texture effects on flow resistance in mobile bed rills. *Catena*, 171, 176-184.

Panagos, P., Borrelli, P., Poesen, J., Ballabio, C., Lugato, E., Meusburger, K., Montanarella, L., Peng W., Zhang Z., Zhang K., 2015. Hydrodynamic characteristics of rill flow on steep slopes. *Hydrological Processes*, 29, 3677-3686.

Peng, W., Zhang, Z., Zhang, K., 2015. Hydrodynamic characteristics of rill flow on steep slopes. *Hydrological Processes*, 29, 3677-3686.

Pohl, M., Alig, D., Körner, C., Rixen, C., 2009. Higher plant diversity enhances soil stability in disturbed alpine ecosystems. *Plant Soil*, 324, 91–102.

Polyakov, V., Stone, J., Holifield Collins, C., Nearing, M.A., Paige, G., Buono, J., Gomez-Pond, R., 2018. Rainfall simulation experiments in the southwestern USA using the Walnut Gulch Rainfall Simulator. *Earth Syst. Sci. Data*, 10, 19–26. https://doi.org/10. 5194/essd-10-19-2018.

Powell, D.M., 2014. Flow resistance in gravel-bed rivers: Progress in research. *Earth-Science Reviews*, 136, 301-338.

Recking, A. Frey, P., Parquier, A., Belleudy, P., Champagne, J.Y., 2008. Bed-load transport flume experiments on steep slopes. *Journal of Hydraulic Engineering*, ASCE, 134, 1302-1310.

Regüés, D., Balasch, J.C., Castelltort, X., Soler, M., Gallart, F., 2000. Relación entre las tendencias temporales de producción y transporte de sedimentos y las condiciones climáticas en una pequeña cuenca de montaña mediterránea (Vallcebre, Pirineos Orientales). *Cuadernos de Investigación Geográfica*, 26, 41–65.

Rosport, M., 1994. Stability of torrent beds characterized by step pool textures. *Int. J. Sediment Research,* 9: 123-132.

Seeger, M., Errea, M.P., Beguería, S., Arnáez, J., Martí, C., García-Ruiz, J.M., 2004. Catchment soil moisture and rainfall characteristics as determinant factors for discharge/suspended sediment hysteretic loops in a small headwater catchment in the Spanish pyrenees. *Journal of Hydrology* 288, 299–311.

Seiz, S.M., Curless, B., Diebel, J., Scharstein, D., Szeliski, R., 2006. A Comparison and Evaluation of Multi-View Stereo Reconstruction Algorithms. *IEEE Conference on Computer Vision ad Pattern Recognition*. IEEE Computer Society, New York.

Smith, M.W., 2014. Roughness in the Earth Sciences. *Earth-Science Reviews*, 136, 202–225.

Song, T., Chiew, Y.M., Chin, C.O., 1998. Effect of bed-load movement on flow friction factor. *Journal of Hydraulic Engineering*, ASCE, 124, 165-175.

Stöcker, C., Eltner, A., Karrasch, P., 2015. Measuring gullies by synergetic application of UAV and close range photogrammetry — A case study from Andalusia, Spain. *Catena,* 132, Pages 1-11. https://doi.org/10.1016/j.catena.2015.04.004.

Stokes, A., Atger, C., Bengough, A.G., Fourcaud, T., Sidle, R.C., 2009. Desirable plant root traits for protecting natural and engineered slopes against landslides. Plant Soil 324, 1–30.

Stolte, J., Tesfai, M., Oygarden, L., Kvaerno, S., Keizer, J., Hessel, R., Panagos, P., Kværnø, S., Verheijen, F.G.A., Ballabio, C., 2016. Soil threats in Europe: status,

methods, drivers and effects on ecosystem services: deliverable 2.1 RECARE project. doi:10.2788/488054.

Strohmeier, S.M., Nouwakpo, S.K., Huang, C.H., Klik, A., 2014. Flume experimental evaluation of the effect of rill flow path tortuosity on rill roughness based on the Manning-Strickler equation. *Catena*, 118, 226-233. https://doi.org/10.1016/j.catena.2014.01.011.

Takken, I., Govers, G., Ciesiolka, C.A.A., Silburn, D.M., Loch, R.J., 1998. Factors influencing the velocity-discharge relationship in rills. Modeling soil erosion, sediment transport and closely related hydrological processes, *IAHS Publ*. 249, 63-69.

Tennekes, H., 1968. Simple Model for the Small-Scale Structure of Turbulence. *The Physics of Fluids*, 11, 669 (1968). https://doi.org/10.1063/1.1691966.

Toy, T.J., Foster, G.R., Renard, K.G., 2002. Soil Erosion: Processes, Prediction, Measurement, and Control. John Wiley & Sons, Inc., New York.

Turowski, J.M., Yager, E.M., Badoux, A., Rickenmann, D., Molnar, P., 2009. The impact of exceptional events on erosion, bedload transport and channel stability in a step-pool channel. *Earth Surface Processes and Landforms*, 34: 1661-1673.

Vanoni, V.A., Nomicos, G.N., 1960. Resistance properties of sediment-laden streams. *Trans. of Am. Soc. Civ. Engrs*., ASCE, 125, 1140-1175.

Verheijen, F.G.A., Jones, R.J.A., Rickson, R.J., Smith, C.J., 2009. Tolerable versus actual soil erosion rates in Europe. *Earth-Science Reviews*, Volume 94, Issues 1–4, Pages 23-38. https://doi.org/10.1016/j.earscirev.2009.02.003.

Vinci, A., Brigante, R., Todisco, F., Mannocchi, F., Radicioni, F., 2015. Measuring rill erosion by laser scanning. *Catena*, 124, 97–108. https://doi.org/10.1016/j.catena.2014.09.003.

Wander, M.M., Yang, Z., 2000. Influence of tillage on the dynamics of loose- and occluded- particulate and humified organic matter fractions. *Soil Biol. Biochem*., 32, 1551–1560.

Wang, X., Yang, Q., Lu, W., Wang, Z., 2011. Effects of bed load movement on mean flow characteristics in mobile gravel beds. *Water Resources Management*, 25, 2781-2795.

Waters, K.A., Curran, J.C., 2012. Investigating step-pool sequence stability. *Water Resour. Res.*, 48 (W07505), 1–20.

Williams, J.R., Berndt, H.D., 1972. Sediment yield computed with universal equation. *Journal of the Hydraulics Division*, Volume: 98, p. 2087-2098.

Wirtz, S., Seeger, M., Ries, J.B., 2010. The rill experiment as a method to approach a quantification of rill erosion process activity. *Zeitschrift für Geomorphologie*, 54: 47-64.

Wirtz, S., Seeger, M., Ries, J.B., 2012. Field experiment for understanding and quantification of rill erosion processes. *Catena*, 91, 21-34.

Wischmeier, W.H., Smith, D.D., 1960. A universal soil-loss equation to guide conservation farm planning. *Transactions 7th int. Congr. Soil Sci.*, 1960 Vol.1 pp. 418-425.

Yalin, M. S., 1992. River Mechanics. Tarrytown, N.Y.: Pergamon.

Yoon, Y.N., Wenzel, H.G., 1971. Mechanics of sheet flow under simulated rainfall. *J. Hydra. Div.*, ASCE 97, 1367–1385.

Zhang, G., Luo, R., Cao, Y., Shen, R., Zhang, X. C., 2010. Correction factor to dye-measured flow velocity under varying water and sediment discharges. *Journal of Hydrology*, 389, 205–213.

Zhang, P., Tang, H., Yao, W., Zhang, N., Xizhi, L.V., 2016. Experimental investigation of morphological characteristics of rill evolution on loess slope. *Catena*, 137, 536-544. https://doi.org/10.1016/j.catena.2015.10.025.

Acknowledgments

During these three years of PhD. course I felt really supported and guided by many people. At the end of this period, I consider my research group as a second family. First and foremost, I am extremely grateful to my supervisor, Professor Vito Ferro, who I would call my “academic father”, for his inestimable advice, guidance, support and patience and for sharing his knowledge and experience during my PhD. course. A special acknowledgment goes also to my co-supervisor and “academic big brother”, Eng. Vincenzo Pampalone, who always helped me and solved my doubts. I would also like to thank deeply the other members of this great research group, Prof. Costanza Di Stefano, Eng. F. Giuseppe Carollo, Dr. Vincenzo Palmeri and Dr. Maria Angela Serio for their presence and additional guidance on my study. I would like to thank my supervisors during the semester studying abroad in US, Prof. Mark A. Nearing and Prof. Mitchell McClaran, for their hospitality and for the once-in-a-lifetime opportunity they gave me staying in Tucson. I would like to thank the coordinator of the PhD. course, Prof. Vincenzo Bagarello, for his endless willingness and patience with us students. I would like to express my enormous gratitude to my family for the love, principles, and education they gave me. Finally, a big thought goes to my girlfriend and my friends. Without their tremendous understanding and encouragement in the past few years, it would be impossible for me to reach all the goals I reached.